First publ. in: Traffic 8 (2007), pp. 523-542

Molecular Identification of 26 Syntaxin Genes and their Assignment to the Different Trafficking Pathways in *Paramecium*

Roland Kissmehl[*,†], Christina Schilde[†], Thomas Wassmer[†], Carsten Danzer, Kathrin Nuehse, Kaya Lutter and Helmut Plattner

Department of Biology, University of Konstanz, PO Box 5560, 78457 Konstanz, Germany
**Corresponding author: Roland Kissmehl, roland.kissmehl@uni-konstanz.de*
[†]These authors contributed equally to this work

SNARE proteins have been classified as vesicular (v)- and target (t)-SNAREs and play a central role in the various membrane interactions in eukaryotic cells. Based on the *Paramecium* genome project, we have identified a multigene family of at least 26 members encoding the t-SNARE syntaxin (*Pt*Syx) that can be grouped into 15 subfamilies. *Paramecium* syntaxins match the classical build-up of syntaxins, being 'tail-anchored' membrane proteins with an N-terminal cytoplasmic domain and a membrane-bound single C-terminal hydrophobic domain. The membrane anchor is preceded by a conserved SNARE domain of ~60 amino acids that is supposed to participate in SNARE complex assembly. In a phylogenetic analysis, most of the *Paramecium* syntaxin genes were found to cluster in groups together with those from other organisms in a pathway-specific manner, allowing an assignment to different compartments in a homology-dependent way. However, some of them seem to have no counterparts in metazoans. In another approach, we fused one representative member of each of the syntaxin isoforms to green fluorescent protein and assessed the *in vivo* localization, which was further supported by immunolocalization of some syntaxins. This allowed us to assign syntaxins to all important trafficking pathways in *Paramecium*.

Key words: exocytosis, Golgi, *Paramecium*, SNAREs, syntaxin

Received 27 November 2005, revised and accepted for publication 23 January 2007, published online 26 March 2007

Trafficking between intracellular membrane compartments is largely mediated by vesicular transport. A high degree of specificity and complexity occurs in the regulation of vesicle budding, docking and fusion. Central to the docking and fusion process are numerous SNARE proteins, which are localized in various intracellular organelle membranes, thereby maintaining integrity and identity of a given intracellular compartment (1–3). SNAREs vary widely in size and structure and share only one homologous sequence, the SNARE motif, that serves as their defining feature. Specific SNAREs present on two opposing membranes interact to form a highly stable '*trans* SNARE complex' whose formation is tightly coupled to membrane fusion (4,5). SNARE complex assembly involves the interaction of coiled-coil domains present in the individual SNARE proteins to form a parallel, twisted four-helix bundle (6–8). Three of the helices are contributed by Q-SNAREs, while the other helix is provided by an R-SNARE (7,9). The structural classification of SNAREs as either 'Q' or 'R' derives from the presence of a highly conserved glutamine or arginine residue in the core of the helical bundle (10), with the Q-SNAREs further subdivided into Qa-, Qb- and Qc-SNAREs (2,3,11). In the majority of intracellular membrane fusion pathways, the three helical domains contributed by Q-SNAREs are present in three distinct proteins (12), one of which, Qa, is provided by syntaxin (10,11). However, in exocytotic membrane fusion, the two other helices (Qb and Qc) are present in a single SNARE protein, SNAP-23/25 (7).

Large efforts have been undertaken to assign SNARE proteins to different trafficking pathways and defined steps of specific pathways in yeast and mammals (1,3,13). In the ciliate *Paramecium*, no syntaxins have been identified so far. The identification of molecules involved in the specificity of membrane interactions in ciliates is interesting because these cells have very complex and well-established trafficking pathways (14,15). The plasma membrane of ciliates possesses several specialized, regularly arranged sites for endocytosis (16,17). Constitutive endo- and exocytosis (18) occurs at coated pits (parasomal sacs), while exocytosis of dense core secretory vesicles (trichocysts) takes place at alternating preformed sites (15,19,20). Phagocytosis of food particles takes place at the cytopharynx and in different stages; phagosomes (food vacuoles) undergo acidification and neutralization, fusion with lysosomes and retrieval of membranes (14,21). Finally, food vacuoles expel indigestible waste materials by exocytosis at the cytoproct (14). There are two additional sites at the dorsal surface of a *Paramecium* cell, through which the paired contractile vacuole system expels excess water from the cytosol (22). Each of these complexes is composed of a central vacuole surrounded by a periodically fusing membrane system of ampullae and collecting radial arms. The latter are connected to the 'spongiome,' a three-dimensional system of tubules with smooth surface or surface decorations that assists sequestering fluid (23).

Studying proteins involved in membrane interactions in a cell with so many different pathways may help to understand the mechanisms underlying membrane recognition, a process that is not yet well understood. Recently, we identified and characterized the SNARE-specific chaperone *N*-ethylmaleimide-sensitive factor (NSF) (24,25) and a multigene family of R-SNAREs (26) in *Paramecium tetraurelia* and we now provide evidence of the existence of a putative interaction partner, the Q-SNARE syntaxin. The identification and characterization of a syntaxin multigene family with at least 26 members and their localization using either green fluorescent protein (GFP) fusion genes or isoform-specific antibodies yielded interesting insights into the complex trafficking pathways of the *Paramecium* cell and allowed us to identify candidates of the secretory pathway including those for the Golgi apparatus and the plasma membrane.

Results

Characteristics of Paramecium *syntaxins*

On the basis of the *Paramecium* sequencing project of the macronucleus (27), we were able to identify and annotate 26 syntaxin coding sequences by manual assembly of single reads during the early steps of the genome project, which were deposited at European Molecular Biology Laboratory Bank under the accession numbers shown in Table 1. Although, except for two, they all lie on different scaffolds in the assembled whole macronuclear genome, most of them cluster in pairs that allow grouping them into 15 subfamilies (Table 1). Within a subfamily, corresponding paralogues contain the same number of introns located at corresponding positions (except intron 3 in *Ptsyx1-1* and intron 2 in *Ptsyx8-2*). The isoforms also reveal a close relationship to each other, with identities of up to 93% on the nucleotide level and even slightly more on the level of amino acid sequence (Table 1). However, between subfamilies the deduced syntaxin proteins differ remarkably, with identities of $\leq$20%, except for the members of the first three subfamilies (Table 1), which were analysed in more detail.

Because cDNA sequences could be obtained for most of the 26 syntaxin genes, we conclude that most of them are expressed (Table 1). The genes encode proteins of 226–315 amino acids with calculated molecular masses ranging between 26.2 and 36.3 kDa (Table 1). Their open reading frames are interrupted by one to seven short introns, which all display the characteristics of *Paramecium* introns, i.e. bordering by 5′-GT and AG-3′ and a size of 20–31 nucleotides (28,29). However, two genes, *Ptsyx6-2* and *Ptsyx13-1*, appear to be pseudogenes because, if translated, both would produce truncated gene products because of the presence of interrupting TGA stop codons in their open reading frames. Although the genes may be transcribed, which at least is true for *Ptsyx*13-1 according to presence of the corresponding cDNA (Table 1), their function still remains to be elucidated.

The domain structure of most of the gene products largely resembles that of syntaxins known from other species (30). Most of them are composed of three putative functional domains, a carboxy-terminal transmembrane region of 16–20 hydrophobic amino acids, which is supposed to anchor the proteins into the target membranes (31), preceded by a characteristic ~60-residue long membrane-proximal region with the propensity to form coiled-coil α-helical structures and, in some cases, an additional α-helical enriched region of ~90–100 residues in the N-terminus (Figure 1). While the coiled-coil domain is present in each of the *Paramecium* syntaxins and contains the typical features of Q-SNAREs, such as a conserved glutamine at the zero layer and heptad repeats of hydrophobic residues (Figure 2), the N-terminal syntaxin domain are conserved only in a subset of *Paramecium* Q-SNAREs (Figure 1).

To make a prediction about the possible function of the different syntaxin genes, we performed a phylogenetic analysis (Figure 3), taking advantage of the fact that functional conservation should be reflected by sequence conservation. The analysis of the evolutionary relationships reveals that many of the *Pt*Syx proteins are clustering together with syntaxin families of well-known intracellular locations and pathways. For example, *Pt*Syx1–3 can be assigned to syntaxins associated with the plasma membrane (Figure 3). Other syntaxin paralogues were predicted to be associated with the endoplasmic reticulum (ER) (*Pt*Syx8) and the Golgi apparatus (*Pt*Syx5). However, no homologues were found for endosomal syntaxins (including early endosome) neither in the genome of *Paramecium* nor in that of its close relative *Tetrahymena thermophila*. Moreover, a large group of *Paramecium* syntaxins (*Pt*Syx7, *Pt*Syx9, *Pt*Syx10, *Pt*Syx11 and *Pt*Syx12) exists, which seems to have no direct counterpart in metazoan cells (Figure 3). Because close orthologues of this group also exist in the *Tetrahymena* genome, the syntaxins of this clade might be involved in more protozoan-typical pathways, such as the complex phagosomal system (14). Another group of ciliate specific syntaxins, *Pt*Syx4-1, *Pt*Syx4-2 and *Pt*Syx6-1, has members in *Paramecium* as well as in *Tetrahymena* and may be involved in another recycling pathway resembling transcytosis (see below).

*Pt*Syx14-1, *Pt*Syx14-2 and *Pt*Syx15-1 in *P. tetraurelia* and *Tt*28413 in *T. thermophila* all cluster with the Qc-SNAREs that are functionally related to the C-terminus of SNAP-25 (32,33). Members of this clade are known to be involved in multiple membrane trafficking events between early and late endosome, *trans* Golgi network (TGN) and the yeast vacuole (13,34,35).

As we are especially interested in SNAREs acting in stimulated exocytosis, the group of *Paramecium* syntaxins clustering with plasma membrane-associated syntaxins was analysed in more detail. The members of the three

Table 1: Molecular characteristics of the syntaxins in *Paramecium tetraurelia*

Gene	Accession number	Scaffold number	DNA				Protein			
			Length (bp)	ORF (bp)	Introns (number)	Identity[a] (%)	Length (aa)	Size (kDa)	Identity[a] (%)	Identity[a,b] (%)
Ptsyx1 1[c]	CR855934	2	1037	888	6	100	295	33.8	100	100
Ptsyx1 2[c]	CR855933	22	1018	894	5	76.9	297	33.6	67.9	67.9
Ptsyx2 1[c]	CR855927	102	1044	894	6	100	297	34.4	100	31.1
Ptsyx2 2	CR855926	40	1038	894	6	90.4	297	34.4	95.0	31.4
Ptsyx3 1[c]	CR855925	94	1040	915	5	100	304	35.0	100	41.9
Ptsyx3 2[c]	CR855924	81	1044	915	5	79.6	304	34.7	77.0	45.6
Ptsyx4 1[c]	CR855923	127	1125	942	7	100	313	36.2	100	14.5
Ptsyx4 2[c]	CR855922	103	1127	948	7	62.4	315	36.3	53.5	12.2
Ptsyx5 1[c]	CR855921	124	892	813	3	100	270	31.8	100	13.9
Ptsyx5 2	CR855920	88	891	813	3	86.0	270	31.7	94.8	13.2
Ptsyx6 1[c]	CR855914	3	807	786	1	100	261	30.8	100	12.8
Ptsyx6 2[d]	CR855980	6	806	120			39	4.8	97.5	1.0
Ptsyx7 1[c]	CR855913	20	914	867	2	100	288	33.4	100	14.9
Ptsyx7 2	CR855919	13	921	870	2	61.4	289	33.8	48.1	13.9
Ptsyx8 1[c]	CR855918	117	837	813	1	100	270	31.6	100	10.1
Ptsyx8 2[c]	CR855917	9	872	825	2	39.9	274	32.2	40.2	8.1
Ptsyx9 1[c]	CR855916	76	863	816	2	100	271	31.6	100	16.9
Ptsyx9 2	CR855915	64	851	804	2	68.1	267	31.5	67.9	16.6
Ptsyx10 1	CR855932	58	891	741	6	100	246	28.3	100	13.5
Ptsyx10 2	CR855931	56	891	741	6	86.4	246	28.2	89.9	13.2
Ptsyx11 1[c]	CR855930	38	787	717	3	100	238	27.7	100	11.5
Ptsyx12 1[c]	CR855929	13	915	867	2	100	288	33.6	100	15.5
Ptsyx13 1[c,d]	CR855928	50	883	363	3		120	14.4		2.0
Ptsyx14 1[c]	gi124392812	11	709	681	1	100	226	26.4	100	6.8
Ptsyx14 2[c]	gi124423260	7	709	681	1	93.1	226	26.2	91.2	7.1
Ptsyx15 1[c]	gi124414298	41	823	798	1	100	265	30.3	100	10.5

ORF, open reading frame; aa, amino acid.
[a]Sequences were aligned by the CLUSTALW method.
[b]Numbers refer to the amino acid sequence of *Pt*Syx1 1.
[c]Genes were analysed also on the cDNA level.
[d]Putative pseudogene.

Paramecium subfamilies *Pt*Syx1, *Pt*Syx2 and *Pt*Syx3 show a higher similarity to each other than to syntaxins from other subfamilies, exhibiting sequence identities of more than 30% on the amino acid level (Table 1). Consequently, secondary structure predictions confirm such a close relationship between the members of these subfamilies, and corroborate their affiliation to the group of plasma membrane-associated syntaxins (Figure 4A). They contain a bundle of three α-helices at the amino-terminal half domain (Habc domain), interspaced with linker regions of variable sizes (Figure 4A). Molecular modelling data (Figure 4B) support the hypothesis that such a conserved autonomously folding structure in the amino-terminal half of the molecule may act as an autoinhibitory regulatory domain, as it is known from the exocytosis-relevant syntaxin 1A (36,37). By folding back onto the membrane-proximal SNARE domain (H3 domain) with the conserved glutamine at the center, the molecule may adopt a 'closed' configuration that would prevent the formation of a core fusion complex with SNARE domains from other SNAREs (Figure 4B). Structural modelling also revealed the coiled-coil conformation typical of a syntaxin SNARE domain (Figure 4C). Attempts of molecular modelling with other members of the *Paramecium* syntaxin subfamilies did not yield any defined structures.

Localization of Paramecium *syntaxins*

To test whether the bioinformatical data correctly predict the compartment or pathway of a given syntaxin, we fused at least one isoform of each subfamily to the *gfp* gene (38) and transformed the macronucleus of *Paramecium* cells. The following results are based on the assumption that the GFP fusion proteins reflect the correct localization of the endogenous proteins. In two cases, for *Pt*Syx1 and *Pt*Syx2, we also used antibodies to confirm the localization of the endogenous protein. Most syntaxins were C-terminally fused to GFP. However, in case of ER retention an additional fusion protein was constructed with the GFP gene fused to the 5′-end of the syntaxin gene (see 'Materials and Methods' section).

GFP-*Pt*Syx1-1 was localized predominantly in the cell cortex, particularly in the plasma membrane, including the numerous sites for constitutive and stimulated

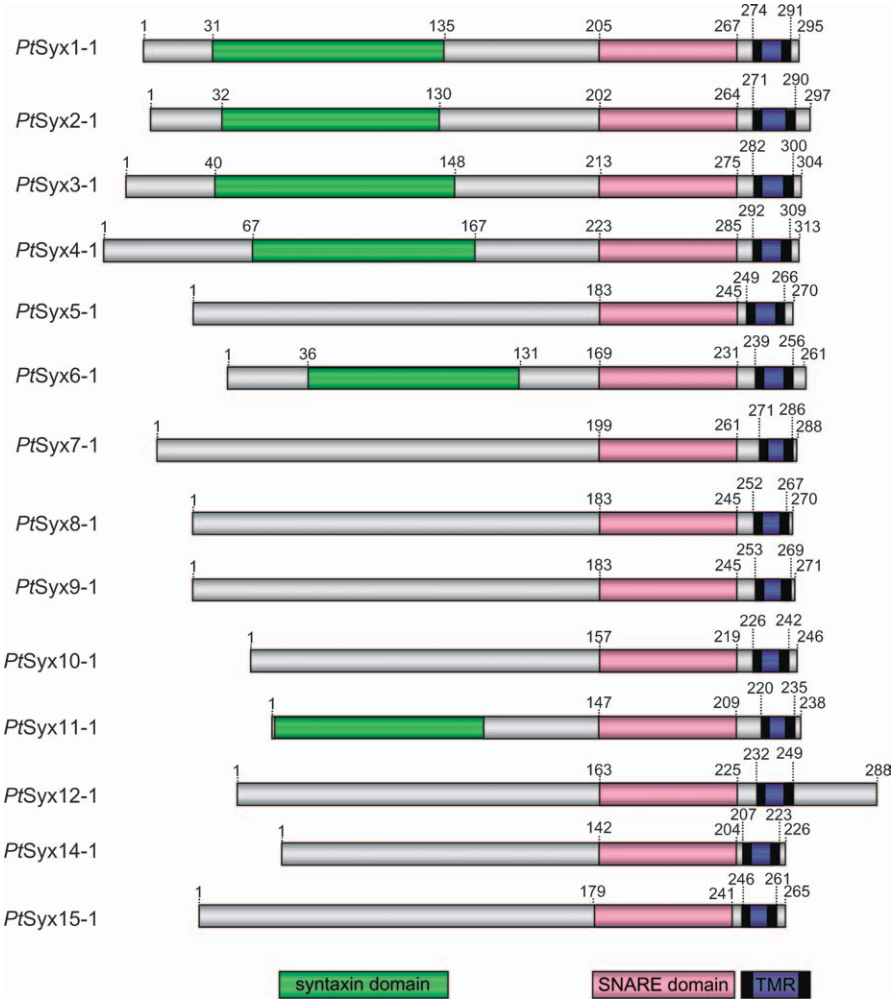

Figure 1: Domain structure of individual members of the *Paramecium* syntaxin superfamily. Results from conserved motif searching are shown for individual members of each of the subfamilies. Characteristic features are the syntaxin domain (green), the SNARE domain (pink) and the transmembrane region (blue/black). Note, the *N* terminal syntaxin domain is not well conserved within the *Paramecium* syntaxins.

exocytosis. This is visible in median sections through a cell (Figure 5A), where fluorescence is concentrated in small spots that are highly regularly arranged over the cell surface (Figure 5A, inset, C, enlargement in D). In dividing cells (Figure 5C), the GFP signal seems to be enriched especially in regions of extensive vesicle traffic underlying the plasma membrane (Figure 5A, inset), including early endosomes (terminal cisternae) near the developing

```
          -7 -6  -5 -4  -3 -2  -1- 0  +1 +2  +3 +4  +5 +6  +7 +8
205 EKYKDIQQLERSVQLVYQLFVDLAILVHAQGQQIDNIEINLDSAKTYVGKAEKSLVDAKEDHQ  PtSyx1-1
207 EKYKDIQQLEKSVQLVFQLQQDLAILVGTQGQITTNIEGSLTSAKSYVNKAKDDLIDAEGDHK  PtSyx1-2
202 DKYQDIQKLEKSTQYCFQMLSEIAFLVNQQGEQIESIEQNLNKAKNYIERGEKRLAKEQEIHK  PtSyx2-1
202 DKYQDIQKLEKSTQYCFQMLSEIAFLVTQQGEQIESIEQNLNKAKNYIEKGEKALAKEQKIHK  PtSyx2-2
213 EKYKDIVKLEKSVQQMYQLFADMAVLVKNQGELIDNIEQNMVKARDYVIKGEDEQRKAKKNHK  PtSyx3-1
213 EKYQDIVKLERSVQQVYQLLVDMAVLVKNQGELIDNIEQNMVKARDYVKKGEAQLVKAKKDHQ  PtSyx3-2
223 ERDQEINKLVTMINELAEVFKSLNQLVIDQGTILDRIDYNIDQAVFNVKKANEELKKAEDYQN  PtSyx4-1
225 ENDQEINKLVKMINDLAQVFQSLNQLVLEQGHLLDRIDENIDQSYKNIKKANHELQESERNQN  PtSyx4-2
183 EKLVSMQKIESMLNDIAGVFQRVGTMVRLQETMIERIDKYTDEAQLNVSKGRKELQESHKRIS  PtSyx5-1
183 EKLVSMQKIESMLNDIAGVFQRVGTMVRLQETMIERIDKYTDEAQVNVSKGRKELQESHKRIS  PtSyx5-2
169 DRNDRIKSLGEKLKKMNELFIEMNRLVIEQGTLLDRIDFNIDQTFTRIQKGKQQLVQANTKQE  PtSyx6-1
199 ERQRELDIIEREALQLNLIVNQMGELTDQQGQELDFGQQNLNEAKANVIGVSNELVGAEENQK  PtSyx7-1
198 ERQKELDDIEREAVQLNLLANQMGSTLGQQGVNLNFGQQNISQVKPKVIQTQNKIVSVDRQQK  PtSyx7-2
183 NEMKDILSIQQQIRDISSSLQRMQEIIAHQEKLTEEIMIQANESLLNIEKGNKHLISATKMNE  PtSyx8-1
187 NDINEIISIKEQISDICLYIQNMQNLIVYQEMKTEEILLNATESFKHIEAANNHLFSSVILNE  PtSyx8-2
183 QNQEDLDKLQMKAYTVNKIVQDLALEIEHQGTIFDEIETNVTTTMVHVVGAGEQLEKIQEQQK  PtSyx9-1
179 QNQEEIDQIQYKTQTINKIVQDLALEIEHQDTYFDVIETNVTTTKENVIKTQDQLTKIQEQQK  PtSyx9-2
157 EQQEEIDQIQKDALEVLKIQTEVAKVVVDQGKMLDVAENNINKSNTNVKEAVVELEGAKVEHK  PtSyx10-1
157 EQQEEIDQIQKDALEVLKIQTEVARVVVDQGKMLDVAENNINVSNKNVKEVVVELEGAKVEHK  PtSyx10-2
147 EREEEIQRIDREAQMLNKLVGELAFEVNKAEEILDIIDVNQKTADQNIKGAIVELDKAQDSQK  PtSyx11-1
163 EKQEEIDTIEKDALLLNRIVNDMSTEVNKQGNQLNEVEMNMTTVQDNLKVTVKELDGAKFEQK  PtSyx12-1
142 EQDQKLDVCIDQLDTLKAQGKNIGNTVDEQNRLLEQIDKDMDKTNKEMINVNGKLKKFLNSSS  PtSyx14-1
142 EQEQKLDVCIDQLDTLKVQSKNIGNTVDEQNRLLGEIEKDMDKTNKEMINVNGKLKKFLNSSS  PtSyx14-2
179 QQDKLLDRTNDQADQLKQQGKQINLTLDEQNKQLDKLNIDVDKTNQQMMTTNNKLVKLIAKSS  PtSyx15-1
```

Figure 2: Sequence alignment of the SNARE domain. The sequence analysis was adapted to the 16 layers (yellow) of the four helix bundle in the synaptic fusion complex (10), including seven layers up stream and eight layers down stream of the ionic layer (layer 0). The conserved glutamine residue forming the ionic 0 layer is indicated in blue. Deviations are shown either in red (layer 0) or in green (other layers).

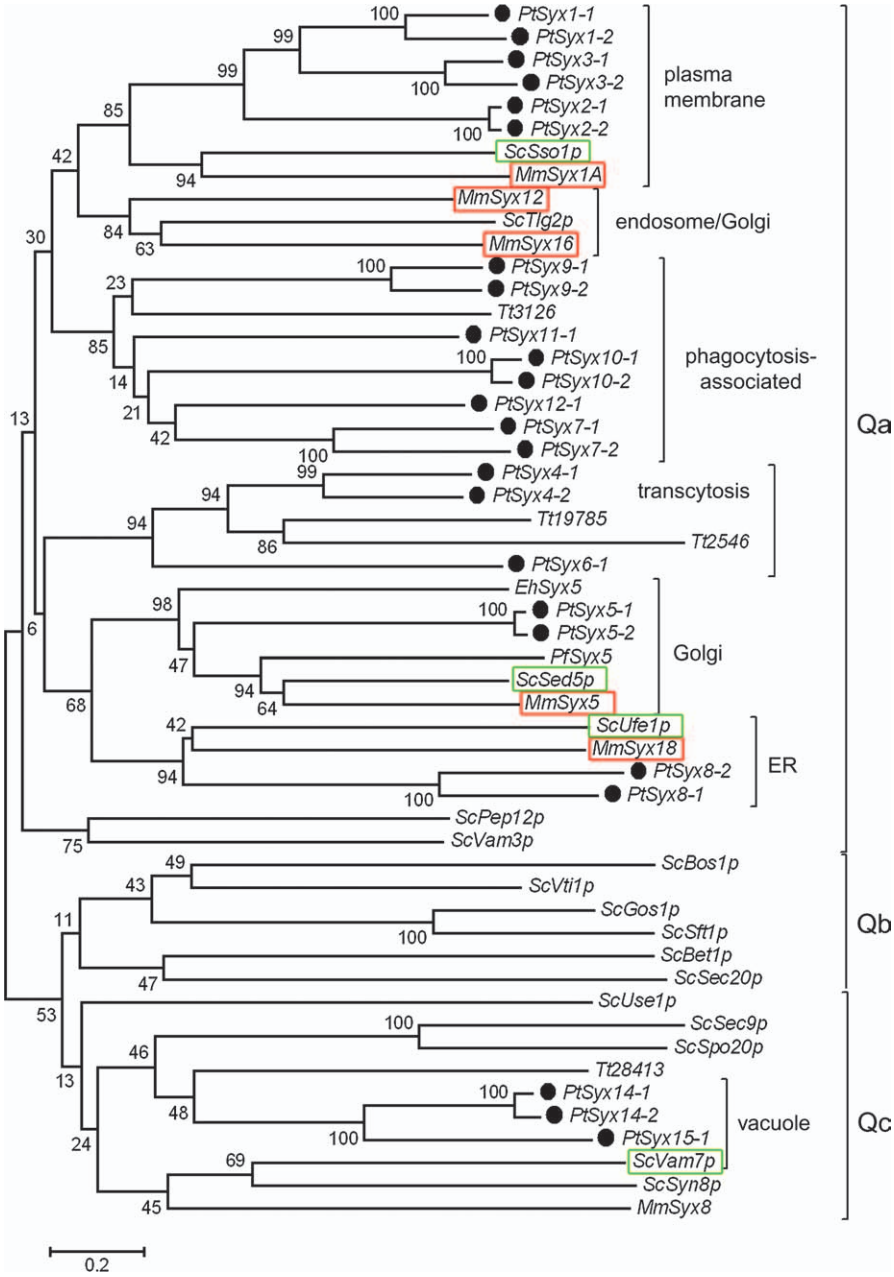

Figure 3: Evolutionary relationships of the *Paramecium* syntaxins with other syntaxins. Predictions from multiple sequence alignments are shown in a neighbour joining tree (with 1000 bootstrap replicates) for an analysis generated with the MEGA version 3.0 program. Besides the *Paramecium* specific SNARE domain coding sequences of syntaxins (*Pt*Syx1 1, *Pt*Syx1 2, *Pt*Syx2 1, *Pt*Syx2 2, *Pt*Syx3 1, *Pt*Syx3 2, *Pt*Syx4 1, *Pt*Syx4 2, *Pt*Syx5 1, *Pt*Syx5 2, *Pt*Syx6 1, *Pt*Syx7 1, *Pt*Syx7 2, *Pt*Syx8 1, *Pt*Syx8 2, *Pt*Syx9 1, *Pt*Syx9 2, *Pt*Syx10 1, *Pt*Syx10 2, *Pt*Syx11 1, *Pt*Syx12 1, *Pt*Syx14 1, *Pt*Syx14 2 and *Pt*Syx15 1) labelled with a filled circle, other syntaxin SNARE domain coding sequences were from *Entamoeba histolytica* (*Eh*Syx5, AAR06581), *Mus musculus* (*Mm*Syx1A, NP 058081; *Mm*Syx5, NP 062803; *Mm*Syx8, NP 061238; *Mm*Syx12, NP 598648; *Mm*Syx16, NP 766263 and *Mm*Syx18, AAH21362), *Plasmodium falciparum* (*Pf*Syx5, CAD52459), *Saccharomyces cerevisiae* (*Sc*Bet1p, P22804; *Sc*Bos1p, AAB67582; *Sc*Gos1p, NP 011832; *Sc*Pep12p, AAB38370; *Sc*Sed5p, NP 013126; *Sc*Sec9p, NP 011523; *Sc*Sec20p, NP 010786; *Sc*Sft1p, NP 012919; *Sc*Spo20p, NP 013730; *Sc*Sso1p, CAA47959; *Sc*Syn8p, NP 009388; *Sc*Tlg2p, NP 014624; *Sc*Ufe1p, AAB50196; *Sc*Use1p, NP 011417; *Sc*Vam3p, AAC49737; *Sc*Vam7p, NP 011303 and *Sc*Vti1p, AAC49745) and *Tetrahymena thermophila* (*Tt*2546, *Tt*3126, *Tt*19785, *Tt*28413). Syntaxin orthologues with characteristic localizations are boxed in red (mouse) or green (yeast). Note that within the Qa SNAREs, there are two clades of protozoan specific syntaxins which seem to have no counterparts in mammalian or other metazoan cells and which may be relevant for phagocytosis and transcytosis, respectively. In contrast, *Paramecium* seems to have neither orthologues assignable to the clades of endosome/Golgi nor any clear Qb syntaxin homologues. Bootstrap support values for the nodes are shown and evolutionary distances are indicated by the scale bar below.

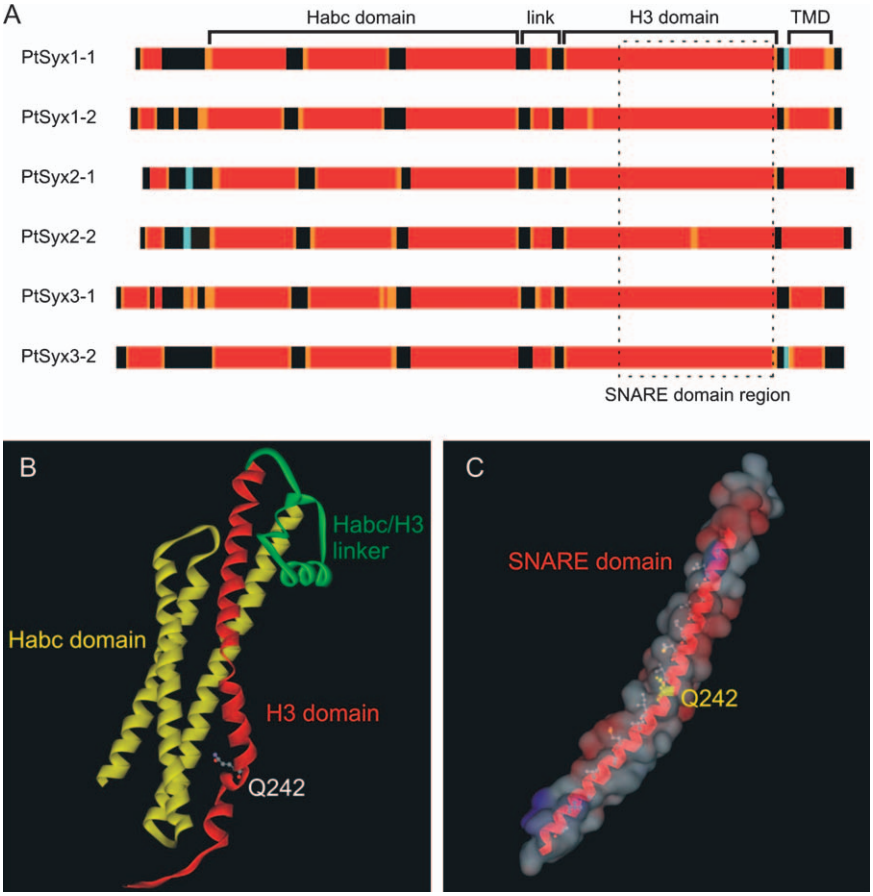

Figure 4: Structure analysis of 'plasma membrane-associated' type of *Pt*Syx protein subfamilies. A) Predicted secondary structure of *Pt*Syx proteins; colored bars represent *Pt*Syx sequences. Red and orange represent regions predicted to form α helical structures with higher (>5) and lower confidence (<5), respectively. Blue, predicted beta strands; black, predicted loops. Secondary structure prediction and confidence levels were assigned by PSIPRED. B) Ribbon representation of *Pt*Syx3 2 modelled via SWISS MODEL 3 5 in 'first approach alignment' mode. The supposed Habc domain is shown in yellow, the Habc/H3 linker in green and the H3 region in red. (C). Electrostatic potentials of *Pt*Syx3 2 SNARE domain region modelled via SWISS MODEL 3 5 in 'first approach alignment' mode. Red, negative potential; grey or white, neutral; blue, positive potential. Q242 (yellow) represents the glutamine of the so called 'zero layer.'

cleavage furrow (between arrowheads). There are also some other specialized regions, such as the most internal part of the cytostome (Figure 5A, enlargement in B) that are brightly stained and from which labelled strings emanate into the cytoplasm, which are quite mobile in living cells. We observed no effect on cell morphology or other physiological aspects by overexpression of GFP-*Pt*Syx1-1.

To support the data from the *in vivo* localization experiments with GFP, we raised a polyclonal antibody against a heterologously expressed *Pt*Syx1-1 peptide and used it in affinity-purified form for several immunoapplications. In Western blots of subcellular fractions from *Paramecium* cells, *Pt*Syx1 can be detected in the 100 000 × *g* pellet and in isolated cortex fractions (Figure 6A). Similarly, a strong immunofluorescence signal occurs in the membranes of isolated cortex fractions (Figure 6B,C). It is especially enriched in the membranes along the outlines of surface fields (kinetids), especially near the intersections of longitudinal and transverse ridges (Figure 6B), however, absent from underlying compartments like alveolar sacs (Figure 6 C). This is further corroborated by immunoelectron microscopic (EM) analysis (Figure 7A–C). Label occurs not only along the cell membrane and on vesicles associated with terminal cisternae (Figure 7A,B) but also on the membranes of discoidal vesicles (Figure 7C), thus being compatible with the *in vivo* localization data obtained with GFP (Figure 5A–D).

*Pt*Syx2-1-GFP is targeted exclusively to the contractile vacuole complex (Figure 5E–H). The protein seems to be present in most membranes of the contractile vacuole system including contractile vacuole, ampullae, radial arms and the 'smooth spongiome' surrounding them. It may act in several fusion and fission events during the pumping cycle, including reversible fusion of the radial arms with the contractile vacuole and of the contractile vacuole with the plasma membrane (Figure 5F,G). Interestingly, when new contractile vacuole complexes are formed at the anterior side of the existing ones during cell division (Figure 5H), these also contain *Pt*Syx2-1-GFP and pulsate.

*Pt*Syx3-1-GFP staining also yields a regular, punctate staining close to the cell surface, resembling that produced by GFP-Syx1-1 (Figure 5I, enlargement in J). Again, the fluorescence signal occurs slightly below the plasma membrane (Figure 5K), where 'terminal cisternae' were suggested to be structures homologous to early endosomes (16). Fluorescence is particularly abundant in the uppermost region of the cytostome (Figure 5L), where parasomal sacs and probably early endosomes are even more concentrated (16).

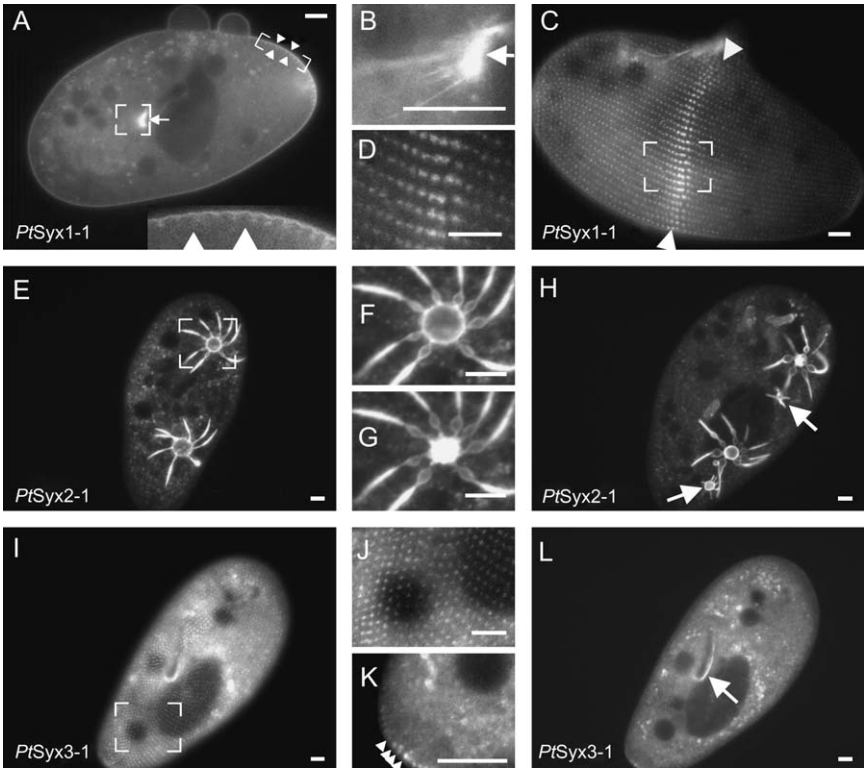

Figure 5: ***In vivo*** **labelling of *Pt*Syx1-1, *Pt*Syx2-1 and *Pt*Syx3-1.** A) In a median section through a cell GFP *Pt*Syx1 1 is enriched at the cell surface (arrowheads). Staining of blisters (A, top) suggests localization in the plasma membrane and underlying terminal cisternae (A, inset; enlargement from area between arrowheads). Some specialized sites of the cytostome (indicated with an arrow) as well as structures associated with fibers emanating from the cytopharynx (enlarged in B) are also stained. C) At the cell surface, GFP *Pt*Syx1 1 fluorescence is concentrated in patches that are regularly arranged along the surface. Staining is most abundant near the fission region (arrowheads), enlargement in (D) of dividing cells. E H) Localization of *Pt*Syx2 1 GFP. The fusion protein is targeted to the contractile vacuole complex where it localizes to the radial arms and the associated spongiome, the ampullae and the contractile vacuole. F) The contractile vacuole before and G) after fluid discharge. H) At an early stage of cell division, when two old contractile vacuole complexes have already doubled, both newly formed complexes contain *Pt*Syx2 1 GFP. I L) Fluorescence of *Pt*Syx3 1 GFP (I, enlarged in K) produces a punctate pattern resembling that of GFP *Pt*Syx1 1, although *Pt*Syx3 1 GFP does not stain the plasma membrane (K). The labelled structures appear to be localized in the cell cortex at a small distance from the plasma membrane (K, arrowheads). In median sections, labelling of the cytopharynx is also visible (L, arrow), suggesting labelling of terminal cisternae. Bars 10 μm.

*Pt*Syx4-1-GFP yields a strong diffuse fluorescence signal in the cytoplasm (Figure 8A,B) and occurs in the membranes of small vesicles that are attached to cytoskeletal elements, along which they are transported. Because the vesicles are very abundant near the cytoproct and along the oral cavity, they may represent discoidal vesicles that retrieve the membranes of spent phagosomes from the cytoproct (14). As vesicles are endocytosed at the cytoproct, transported through the cytoplasm and finally fuse with the plasma membrane at the cytopharynx, the process strongly resembles transcytosis. This trafficking pathway is known to involve syntaxins in epithelial cells (39,40).

GFP-*Pt*Syx5-1 appears in several hundred, ~1- to 1.5 μm-long and <1 μm wide, rod- or banana-shaped organelles per cell (Figure 9A,B), that are enriched in the cell cortex in non-dividing cells (compare Figure 9A, surface, and C, median section). However, in dividing cells, these structures are more equally distributed throughout the cell (Figure 9D). A similar pattern of fluorescence label was found in cells expressing a GFP fusion of the R-SNARE *Pt*Sec22 (Figure 9E–H). Because Sec22 is known to shuttle in different SNARE complexes between ER and Golgi (41,42), a less distinct pattern of ≥1 μm particles compared to GFP-*Pt*Syx5-1 was found (Figure 9F). Like for GFP-*Pt*Syx5-1, those structures were also enriched in the cortical regions of non-dividing cells (Figure 9G) and assumed an even distribution during cytokinesis (Figure 9H). Immuno-gold EM analysis of GFP-*Pt*Syx5-1-expressing cells identified these structures as Golgi elements (Figure 10A) and a similar labelling associated with Golgi cisternae was found for GFP-*Pt*Sec22 (Figure 10B). However, in the immuno-EM analysis of GFP-*Pt*Sec22 cells, the Golgi cisternae appeared to be expanded, possibly as a result of overexpression of the GFP-fused Sec22 protein, which could interfere with ER–Golgi trafficking. Because *Pt*Syx5-1 and *Pt*Syx5-2 cluster in the phylogenetic analysis

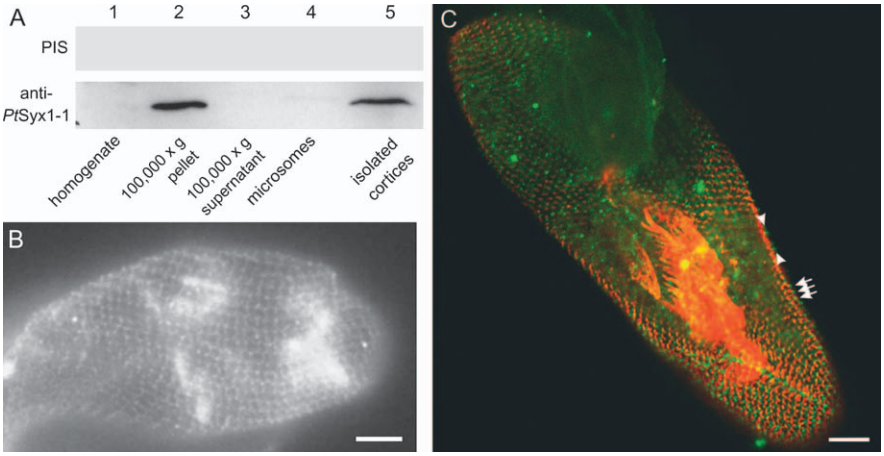

Figure 6: Immunolocalization of the *Pt*Syx1 subfamily using affinity-purified antibodies against *Pt*Syx1. A). Western blot analysis of the subcellular distribution of *Pt*Syx1. In lanes 1 5 aliquots (50 μg) of cell homogenates, 100 000 × *g* pellet, 100 000 × *g* supernatant, microsomes and isolated cell cortices were processed for immunoprobing using either preimmune serum (PIS, top) or affinity purified antibodies against a recombinant peptide representing the region between I_{82} I_{210} of *Pt*Syx1 1 (bottom). Members of the *Pt*Syx1 subfamily occur in the pellet fraction (lane 2), especially in the cortex of a *Paramecium* cell (lane 5). B) Immunofluorescence analysis of *Pt*Syx1. Isolated cortices were incubated with antibodies against *Pt*Syx1, followed by fluorescein isothiocyanate coupled goat anti rabbit IgGs. By using the same polyclonal antibody as in (A), a strong fluorescence signal occurs in the membrane along the outlines of surface fields (kinetids), predominantly near the intersections of longitudinal and transverse ridges. C) Double labelling of *Pt*Syx1 and tubulin in isolated cortices. These were processed for *Pt*Syx1 staining (green) as in (B) and co incubated with a monoclonal anti tubulin antibody (red) that predominantly stains basal bodies. Note that *Pt*Syx1 label is located slightly above basal bodies (between arrowheads), suggesting its localization at the plasma membrane. Bar 10 μm.

with Golgi-specific syntaxins of other organisms (Figure 3) and GFP labelling of *Pt*Syx5-1 is compatible with a localization in the Golgi apparatus of *Paramecium* (Figure 9), we asked whether the GFP-labelled structures in *Paramecium* can be disassembled by Brefeldin A (BFA), as would be expected from the results of other systems (43). Therefore, BFA was applied to GFP-*Pt*Syx5-1-transfected cells and the effect on the fluorescence signal was monitored at varying time points (Figure 11). Indeed, the rod- or banana-shaped, cortically enriched organelles disappeared upon treatment with BFA, and instead brightly labelled patches appeared (compare Figure 11A with B and C). This process was reversible, as shown by washout of BFA, leading to the reassembly of the original organelles (Figure 11D).

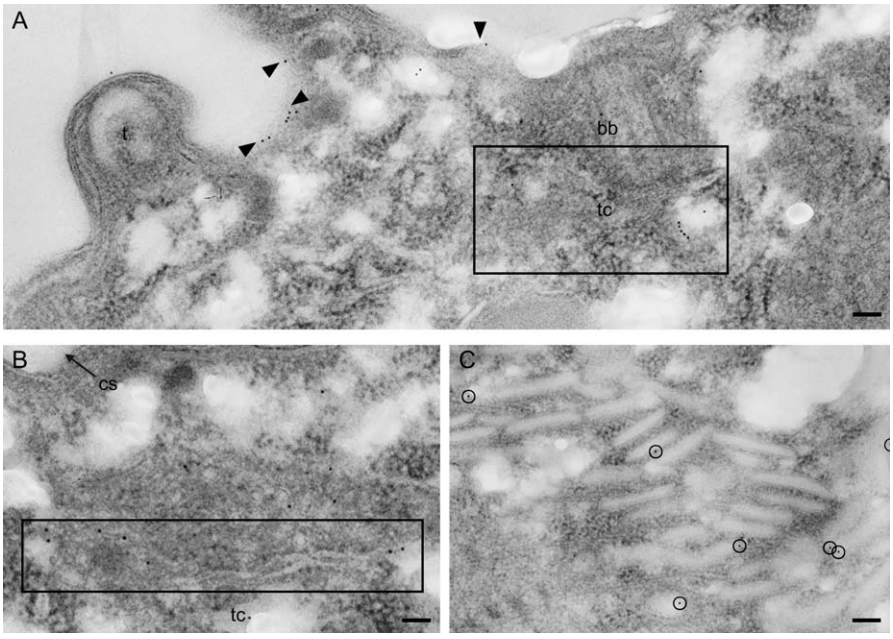

Figure 7: Immuno-gold EM localization of *Pt*Syx1-1-GFP. Sections labelled with anti GFP antibodies, followed by pA Au_5. A) Note label along the cell membrane (arrow heads) particularly along a 'grazing' section part between arrowheads, as well as labelling of vesicles asso ciated with a terminal cisterna (tc) within the framed area. B) Labelling associated with a tc below the cell surface (cs) inside framed area. C) Labelling of discoidal vesicles (circles). bb, basal body; t, trichocyst. Bars 0.1 μm.

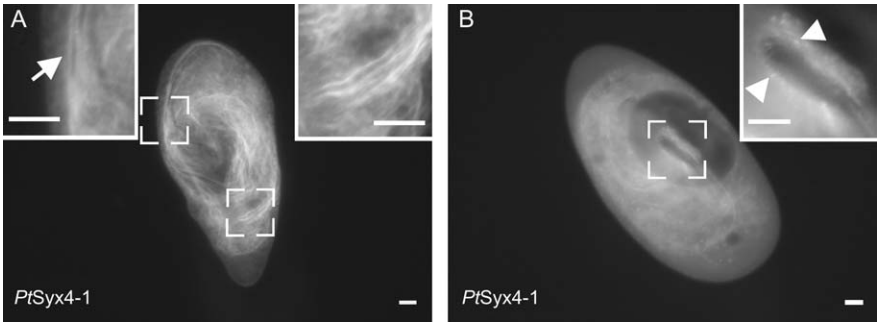

Figure 8: *In vivo* labelling of *Pt*Syx4-1. *Pt*Syx4 1 GFP brightly stains cytoplasmic elements, presumably membranes of very small vesicles travelling along cytoskeletal elements (A,B) according to movies (data not shown). A) Enlargements. These vesicles are enriched near the cytoproct (arrow) as well as along the oral cavity (B, enlargement), where vesicles are faintly visible (arrowheads). Note that the anterior pole of the cells (bottom in A, top in B) is devoid of any label. Bars 10 μm.

However, higher concentrations than described for animal cells had to be used for prolonged periods, probably because of differing penetration and pharmacological sensitivity. For comparison, in plant cells BFA had to be applied at a concentration of 50 μg/mL for 30 min to achieve the redistribution of *Arabidopsis thaliana At*Sec22 and *At*Membrin from Golgi bodies to the ER membranes (44). We obtained similar results when we treated GFP-*Pt*Sec22-transfected cells (Figure 11E) with the same concentration of BFA, i.e. upon treatment a complete redistribution of label to an ER-like pattern was found (Figure 11F). Again, this effect was reversible and after washout of BFA the staining assumed a cortically enriched particulate pattern again (Figure 11G). This experiment demonstrates that the integrity of these organelles and distribution of marker proteins is clearly affected by BFA and this further argues for presence of *Pt*Syx5 and *Pt*Sec22 in and near the Golgi apparatus, respectively. This effect is specific for the Golgi-localized *Pt*Syx5 and *Pt*Sec22 because other syntaxins, like *Pt*Syx2 of the contractile vacuole system, are not affected in their localization by treatment with BFA (Figure S1).

For unknown reasons, neither N- nor C-terminal GFP fusion constructs of *Pt*Syx6-1 gave fluorescence signals in living or fixed cells (not shown), although we found that *Pt*Syx6-1 is expressed according to the presence of its cDNA (Table 1).

*Pt*Syx8-2-GFP mainly stains reticular structures in the cytoplasm (Figure 12A). By focussing on the cell cortex, the labelled structure appears to be ER, as it resembles the pattern after ER affinity staining with $DiOC_6$ or $DiOC_{18}$ (45,46). Furthermore, the *Pt*Syx8-2-GFP staining overlaps with the ER-localized synaptobrevin *Pt*Syb3 (26) as shown by confocal imaging of co-staining with the respective antibody (Figure 12B–E). This co-staining occurs especially in the cortical regions of ER.

*Pt*Syx7-2-GFP is transported to phagosomes, but it also stains the cytoplasm, probably because of its presence in the membranes of small vesicles (Figure 13A,B). Only a small fraction of phagosomes contain *Pt*Syx7-2 in their membranes, suggesting that food vacuoles at different stages of maturation differ in their membrane composition, as discussed by Allen and Fok (14) and therefore possibly also in their set of SNAREs.

GFP-*Pt*Syx9-1 is also localized in small vesicles dispersed throughout the cytoplasm (Figure 13C,D). Interestingly, in the case of *Pt*Syx9-1-GFP, where the GFP tag was C-terminal and exposed to the lumen of the vesicle, the fusion protein does not produce any fluorescence signal in the living cell. However, fluorescence appears after fixation with formaldehyde, leading to fields of fluorescent vesicles (not shown). Because the enhanced version of GFP we used [eGFP, (37)] does not fluoresce at pH $<$ 5 (47) and becomes visible only after fixation, it is most likely that vesicles containing *Pt*Syx9-1-GFP are acidic.

*Pt*Syx10-1-GFP resides in vesicles with a size range of 1–2 μm (Figure 13E,F) that are travelling rapidly with the cyclosis stream (data not shown). *Pt*Syx11-1-GFP is present in the membranes of most food vacuoles (Figure 13 G,H), while *Pt*Syx12-1-GFP fluorescence is concentrated in 'large patches' and only occasionally occurs on the membranes of food vacuoles (Figure 13I,J).

As a predicted Qc-SNARE, *Pt*Syx14-1-GFP is localized within the ampullae and the radial arms of the contractile vacuole complex (Figure 14A,B) as was observed also for *Pt*Syx15-1-GFP (Figure 14C,D). However, both constructs also produce a diffuse signal in the cytoplasm (Figure 14A–D), probably because of their presence in the membranes of numerous small vesicles.

Functional studies on individual syntaxins of the secretory pathway

To investigate the function of individual syntaxins, e.g. of the secretory pathway, we have performed gene silencing using an RNAi approach by feeding transformed bacteria (48). If the nucleotide identity between the pairs of one

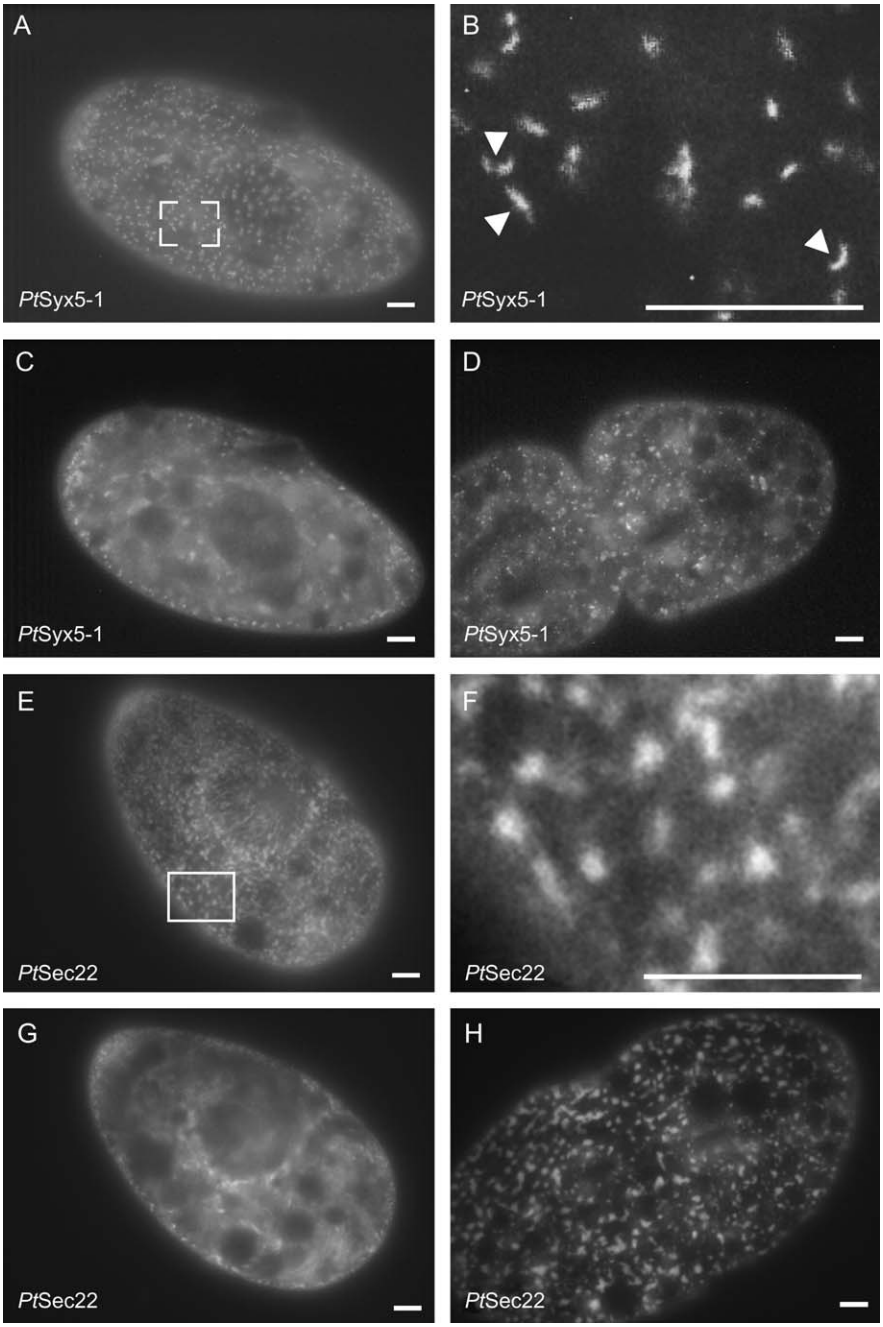

Figure 9: Green fluorescent protein labelling of *Pt*Syx5-1 and *Pt*Sec22. GFP *Pt*Syx5 1 stains ~1 to 1.5 μm long, straight or banana shaped organelles (A, arrowheads in enlargement B). In exponentially growing cells, these are most abundant in the cortical region (C), while in dividing cells they assume a more even distribution throughout the cytoplasm (D). GFP *Pt*Sec22 appears in similar ~1 to 2 μm sized structures, but irregular shaped structures (E, enlarged in F) that are enriched in the cortex region (G) and distribute evenly in dividing cells (H). Because of the shuttling of Sec22 in small vesicles between ER and *cis* Golgi, the staining appears less distinct compared to GFP *Pt*Syx5 1. Bars 10 μm.

subfamily is high enough (≥85%), one can expect co-silencing of isoforms (49). In most cases, we constructed a silencing plasmid specific for just one of the two isoforms (Table 2). For silencing more than one isoform, we used a novel strategy by cloning the complete open reading frame of each isoform in tandem between the T7 promoters of the same feeding plasmid (see 'Materials and Methods' section). As a control for successful gene silencing, we used the established construct targeting *nd7* that results in a non-lethal exocytosis-minus phenotype (49). For mock silencing, either the empty vector pPD or pPD-*gfp* was used. Unfortunately, most of our gene silencing constructs that were targeting only one of the isoforms gave rise to normal phenotypes (Table 2). This argues for a functional overlap between isoforms of the syntaxin subfamilies. For instance, when we used a ~300 bp fragment of genomic DNA for silencing of *Ptsyx1-1* or *Ptsyx1-2*, no phenotypic defects were observed (Table 2). In cells silenced with a construct containing the entire open reading frame of *Ptsyx1-1*, an inhibition of stimulated exocytosis to varying extent was found. Only when we used a double silencing construct containing the full-length open reading frames of both genes (pPD-*syx1-1*$_{ORF}$-*syx1-2*$_{ORF}$), we could observe phenotypic defects (Figure 15;

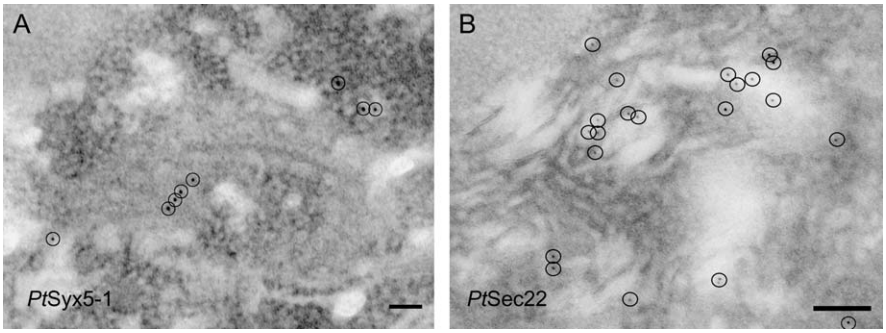

Figure 10: Immuno-gold EM localization of GFP-*Pt*Syx5-1 and GFP-*Pt*Sec22. A) Section of a GFP *Pt*Syx5 1 expressing cell, labelled with anti GFP antibodies, followed by pA Au_5 gold particles (5 nm; encircled). Note labelling of Golgi associated vesicles. B) Same immuno gold anti GFP labelling of pA Au_3 ~3 nm (circles) in a GFP *Pt*Sec22 expressing cell. Note that Golgi stacks appear slightly enlarged possibly as a cause of overexpression of *Pt*Sec22. Bars 0.1 μm.

Table 2). Down-regulation of *Ptsyx*1-1 in Syntaxin1-RNAi cells could be shown by reverse transcriptase–polymerase chain reaction (RT–PCR) using a primer pair with one primer lying outside the open reading frame contained in the silencing construct (Figure 15A). The growth rate of Syntaxin1-RNAi cells was strongly reduced, without the appearance of cells arrested in certain division stages (Figure 15B). Compared to mock-silenced control cells (Figure 15C), the stimulated exocytosis of trichocysts is inhibited in Syntaxin1-RNAi cells (Figure 15D). This effect does not seem to be caused by a defect in trichocyst synthesis or lack of docking because docked trichocysts could be found in controls as well as in Syntaxin1-RNAi cells. However, the inhibition of stimulated exocytosis was never as complete as seen for control nd7-RNAi cells. Further analysis showed that Syntaxin1-RNAi cells are smaller and possess altered proportions as seen as a decreased width:length ratio (Figure 15E,F). Note that the observed reduced exocytosis rate in Syntaxin1-RNA1 cells was not an effect of the reduced cell size because it was measured as percentage of exocytosis per cell and not per surface area.

In *Pt*Syx2-RNAi cells, only a transient reduction of growth rate during the first 24 h of feeding was observed (Table 2). Because *Pt*Syx2 was found in the contractile vacuole complex (Figure 5E–H), it is conceivable that this was an effect on osmo- and/or ion regulation because at the beginning of feeding cells are transferred into a different medium and fed with a different type of bacteria. This finding requires further investigation for instance under osmotic stress conditions.

Discussion

General aspects

Here, we describe 26 syntaxin genes in *P. tetraurelia*, of which 23 should represent the entire set of Qa-SNAREs; the remaining three represent Qc-SNAREs. Most remarkably, no syntaxins of the Qb type were found, which are present in all other systems where the full set of Q-SNAREs is known (11,13,50–52). This function may be performed solely by a SNAP-like Qb/c SNARE, which we also identified (data not shown). The number of syntaxins is much smaller in other unicellular eukaryotes, such as *Plasmodium falciparum* (http://www.plasmodb.org), *Leishmania major* (52), *Giardia*, *Trypanosoma* and some less-studied protozoan parasites (50,53). The *Saccharomyces cerevisiae* and *Drosophila melanogaster* genomes contain only seven Qa-SNARE genes (11,13), while the *Caenorhabditis elegans* genome comprises nine (11), the human twelve (11), and *A. thaliana* 18 Q-SNAREs of the syntaxin type (51). The large number of Qa-SNAREs in the *Paramecium* genome may be explained by a recent global genome duplication event (27) and by the complex membrane trafficking pathways (Figure 16). Mammalian systems increase the number of isoforms by alternative splicing of syntaxins (30,54), with either differential expression or localization (55,56), whereas alternative splicing is not known from *Paramecium*.

Most of the *Paramecium* Qa-SNAREs contain the typical features of syntaxins (Figures 1 and 2), with a SNARE motif for four-helix bundle formation (7,8,33) and a conserved glutamine for NSF-mediated disassembly (57). However, *Pt*Syx11 does not contain the typical glutamine of Q-SNAREs (Figure 3). Such deviations have been described for the equally AT-rich genomes of *Plasmodium* and *Eimeria* (50). Some of the *Pt*Syx, especially the plasma membrane-associated ones, also reveal an autonomously folding N-terminal domain (Figure 4) - a characteristic feature within this clade of syntaxins (36,37). This domain may regulate SNARE assembly by forming a three-helix bundle (Habc) which folds back onto the SNARE domain (58,59). The N-terminal Habc domain may also bind auxiliary proteins like the Sec1/Munc-18 proteins (60,61).

Pt*Syx1-1 as an exocytosis-relevant Qa-SNARE*

We suggest *Pt*Syx1-1 to be the Qa-SNARE relevant for constitutive and stimulated exocytosis for the following reasons. (i) In our phylogenetic analysis, not only *Pt*Syx1-1 and *Pt*Syx1-2 but also *Pt*Syx2 and *Pt*Syx3 can clearly be

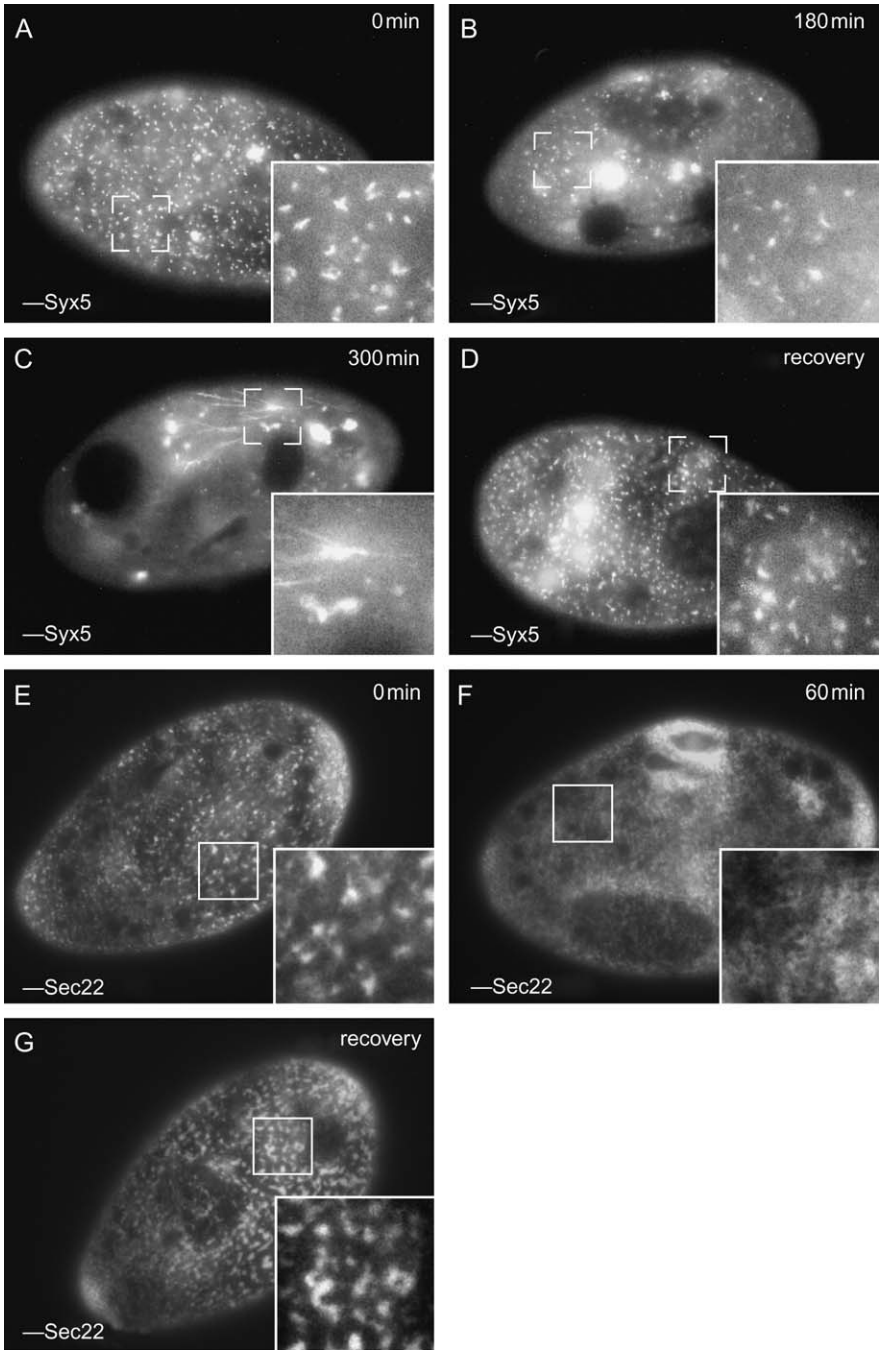

Figure 11: Effect of Brefeldin A on GFP-*Pt*Syx5-1- and GFP-*Pt*Sec22-transfected cells. A) Before BFA treatment, GFP *Pt*Syx5 1 cells show distinct distribution of ~1 μm large, rod to banana shaped organelles. B) After BFA treatment, the number of those small organelles drastically de creases, while strongly stained patches arise in the cytoplasm (C) until eventually none of the original organ elles remain. Instead, labelled strings occur in addition to the large patches. D) After washout of BFA, the pattern of the original organelles has reformed. E) Before BFA treatment, GFP *Pt*Sec22 cells show a distinct distribution of mostly ~1 μm large, irregular shaped structures. F) After BFA treatment, the staining appears in a diffuse, ER like pattern. G) This effect was reversible: after washout of BFA, the pattern of the original organelles could be restored. Bars 10 μm.

assigned to the clade of syntaxins associated with the plasma membrane (Figure 3). Their close relationship (Table 1) also becomes evident from secondary structure predictions, all showing features of plasma membrane-associated syntaxins (Figure 4A,B). This includes possible intermolecular interaction of the Habc domain with the membrane-proximal SNARE domain (H3 domain), as described for other exocytotic syntaxins. (ii) *Pt*Syx1 subfamily members are found in the cell cortex and some specialized regions at the cytopharynx (Figure 16). (iii) Only silencing of *Ptsyx*1 gene family showed an effect on stimulated exocytosis (Table 2, Figure 15D). Those Syntaxin1-RNAi cells furthermore showed a reduced growth rate and cell size, which is in agreement with the localization we found for the GFP-tagged *Pt*Syx1-1 at the fission zone (Figure 5C).

In *Paramecium*, the sites for constitutive exocytosis and endocytosis are at the same place (14,18). The so-called parasomal sacs are permanent omega-shaped indentations of the plasma membrane regularly arranged over the somatic surface of the cell (16) with extensive membrane trafficking to the underlying 'terminal cisternae'

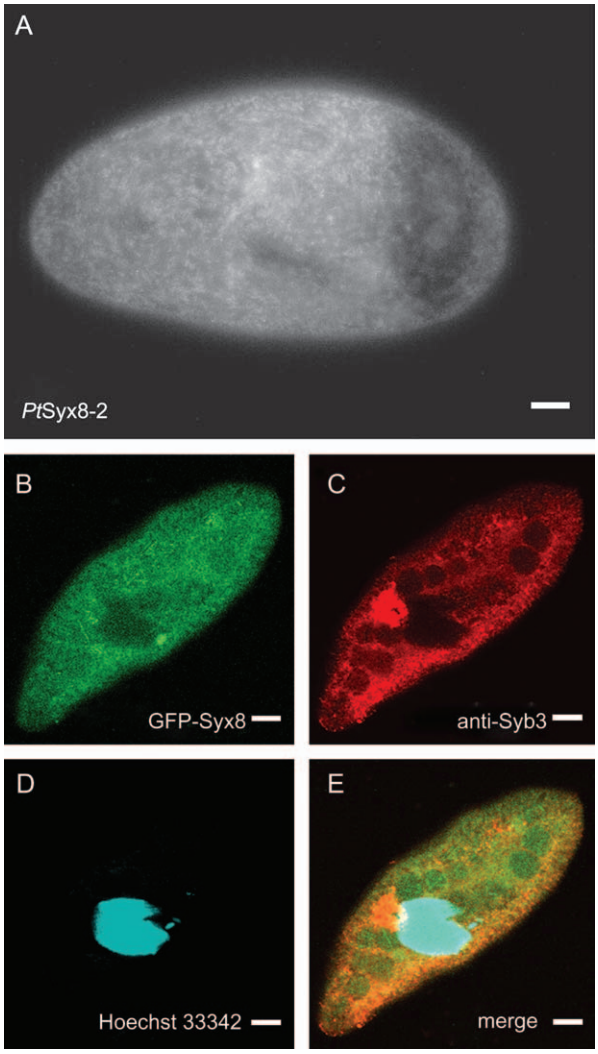

Figure 12: Green fluorescent protein labelling of *Pt*Syx8-2 and colocalization with *Pt*Syb3. A) *Pt*Syx8 2 GFP shows cyto plasmic staining in a 'patchy' manner, with some more distinct structures, e.g. in a tubular form in the cell cortex, all suggesting localization to the ER. (B E) Confocal image slice (1 μm) of a *Pt*Syx8 2 GFP expressing cell co stained with an antibody rec ognizing the established ER resident protein *Pt*Syb3. E) Especially in the cortical regions, there is a high level of colocalization of the two markers. Note that autofluorescence of food particles in food vacuoles produced a background signal in the green channel. Bars 10 μm.

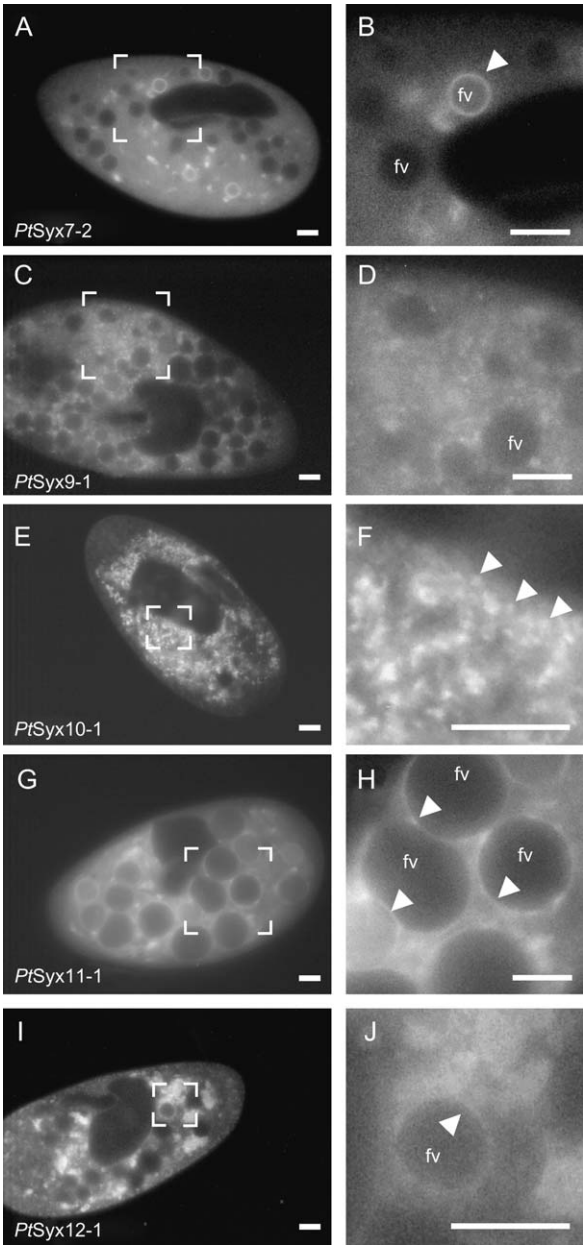

Figure 13: *In vivo* labelling of *Pt*Syx7-2, *Pt*Syx9-1, *Pt*Syx10-1, *Pt*Syx11-1 and *Pt*Syx12-1. (A,B) *Pt*Syx7 1 GFP labels some, but not all food vacuoles (fv) and produces diffuse labelling of the cytoplasm. (C,D) GFP *Pt*Syx9 1 stains small vesicles throughout the cytoplasm, which in some regions are grouped around food vacuoles (see inset, D). (E,F) *Pt*Syx10 1 GFP localizes to vesicles (arrows, F) of ~1 2 μm size that rapidly travel with the cyclosis stream (not shown). (G,H) *Pt*Syx11 1 GFP localizes to membranes of food vacuoles, but, like *Pt*Syx7 1 GFP, it is not associated with all of them. Also note staining of the cytoplasm. (I,J) *Pt*Syx12 1 GFP is found on food vacuole membranes (arrowhead) but also in patches in the cytoplasm. Bars 10 μm.

(14,17,18). For specific membrane recognition, each of these compartments in correspondence may have to be equipped with a unique Qa-SNARE (Figure 5). Immunostaining techniques (Western blots, immunofluorescence, and immuno-EM) independently confirmed the localization of *Pt*Syx1-1 as a GFP fusion protein (Figures 6 and 7). So far, all data strongly suggest *Pt*Syx1-1 being the best candidate for an exocytosis-relevant Qa-SNARE in *Paramecium*. Its function seems to include other pathways originating from the plasma membrane, e.g. the formation of the nascent food vacuole (Figure 5A,B; Figure 16). Because GFP fluorescence is absent at later phagosomal stages, a recycling pathway can be assumed, involving the

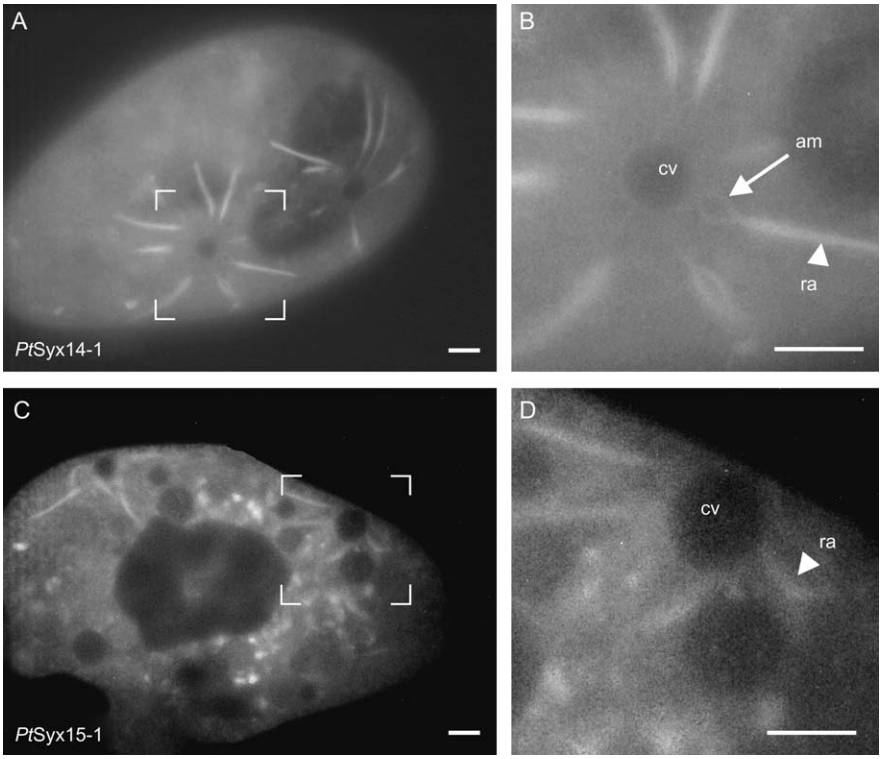

Figure 14: *In vivo* labelling of *Pt*Syx14-1 and *Pt*Syx15-1. Both, *Pt*Syx14 1 GFP and *Pt*Syx15 1 GFP, localize to membranes of the contrac tile vacuole complex, i.e. contractile vacuole (cv), specifically to ampullae (am) and radial arms (ra). Also note some diffuse cytoplasmic staining and brighter patches that might rep resent crystalline inclusions of the cell. Bars 10 μm.

cytopharyngeal ribbons to transport the vesicles back to the cytostome (14). The staining of *Pt*Syx1-1 associated with terminal cisternae in Figure 5A (inset) and in the immuno-EM (Figure 7B) suggests an additional role of *Pt*Syx1 in the endocytic pathway. *Pt*Syx1 may also operate at the contractile vacuole–plasma membrane interface, where it is in recurring contact with the plasma membrane (23). In contrast, paralogues of the *Pt*Syx2 subfamily occur predominantly in the contractile vacuole complex and those of the *Pt*Syx3 subfamily at the early endosome (Figure 16). The localization of putative plasma membrane-associated syntaxins in these organelles may give rise to speculation about their molecular identity and biogenesis. All these data agree with the presence of plasma membrane-associated syntaxins in intracellular compartments in mammalian systems (62–64).

Table 2: Effects of RNAi of individual syntaxin members on cell morphology and various physiological aspects

Construct[a]	Stimulated exocytosis	Morphology	Division rate	Identity to sister isoform (%)
pPD *Pt*syx1 $1_{256–566}$	Normal	Normal	Normal	73.3
pPD *Ptsyx*1 1_{ORF}	Partially inhibited[b]	Normal	Normal	76.9
pPD *Ptsyx*1 $2_{81–337}$	Normal	Normal	Normal	66.1
pPD *Ptsyx*1 1_{ORF} *Ptsyx*1 2_{ORF}	Inhibited	Smaller	Reduced	100
pPD *Ptsyx*2 $1_{264–526}$	Normal	Normal	Normal	89.0
pPD *Ptsyx*2 1_{ORF}	Normal	Normal	Normal	90.4
pPD *Ptsyx*2 1_{ORF} *Pt*syx2 2_{38-897}	Normal	Normal	Delayed (within the first 24 h)	100
pPD *Ptsyx*3 $1_{251–550}$	Normal	Normal	Normal	78.3
pPD *Ptsyx*4 $1_{569–782}$	Normal	Normal	Normal	63.1
pPD *Ptsyx*5 $1_{362–664}$	Normal	Normal	Normal	85.1
pPD *Ptsyx*8 $1_{286–583}$	Normal	Normal	Normal	51.7
pPD *nd7*	Inhibited	Normal	Normal	
pPD (empty vector)	Normal	Normal	Normal	
pPD *gfp* (mock silencing)	Normal	Normal	Normal	

[a]Numbers refer to the base pairs of the macronuclear DNA from which the fragment was created; ORF designates the entire open reading frame was used.

[b]*n* 40 cells; 10 cells were 100% inhibited, 12 cells were 50 75% inhibited and 6 cells 25 50% inhibited; 12 cells were not inhibited.

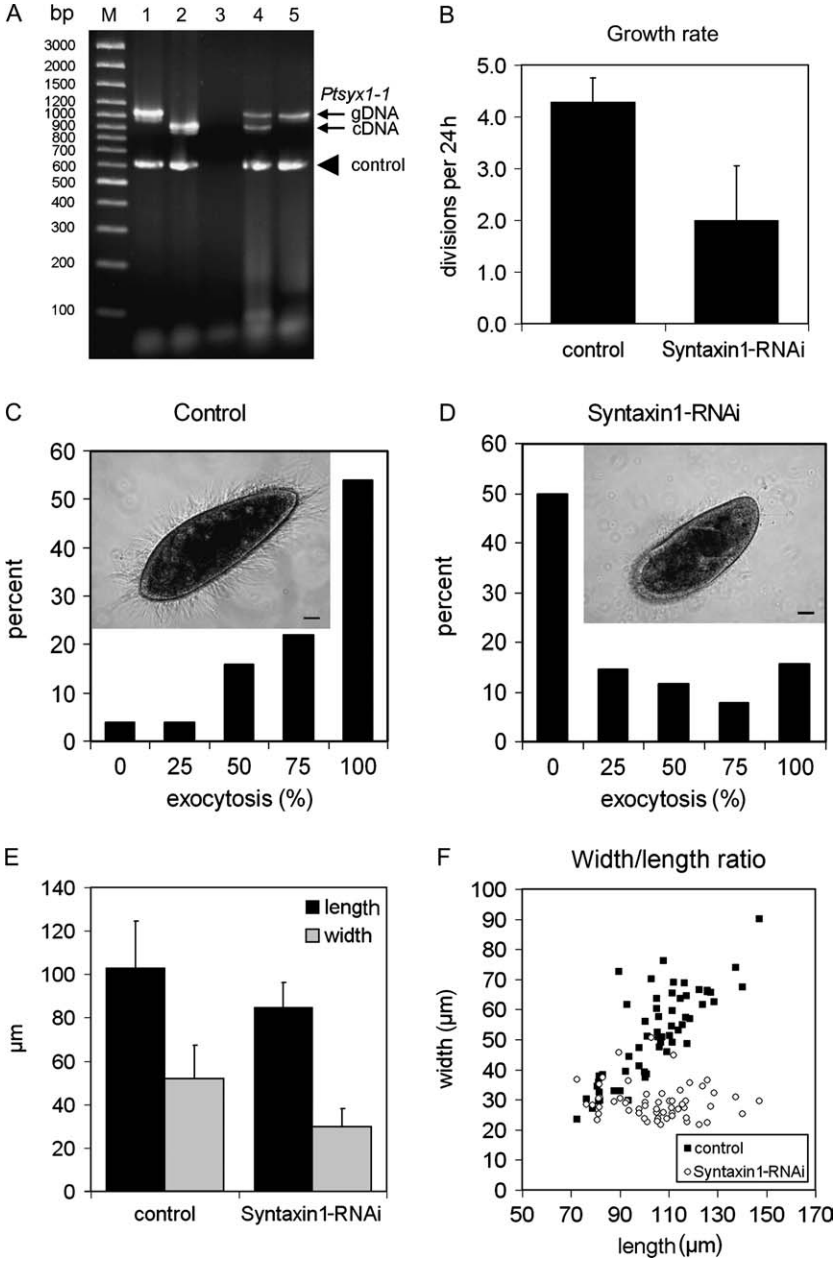

Figure 15: Effects of *Pt*Syx1-RNAi. A) Polymerase chain reaction of *Ptsyx1 1* with a pair of primers with one primer lying outside and the other inside the open reading frame from control macronuclear DNA (lane 1), control cDNA library (lane 2), the silencing plasmid pPD *syx1 1*$_{ORF}$ *syx1 2*$_{ORF}$ (lane 3), not DNAse treated cDNA of pPD *gfp* mock silenced (lane 4) and *syx1* silenced cells (lane 5). No *Ptsyx1 1* could be amplified from the silencing plasmid con trol (lane 3). *Ptsyx1 1* genomic DNA (gDNA), but no cDNA of *Ptsyx1 1* could be amplified from Syntaxin1 RNAi cells (lane 3), whereas a control gene (arrow head) was amplified from all samples except the plasmid (lane 3). Note that the ~600 bp control gene only contains a sin gle 25 bp insert and hence the molecular weight difference between the genomic DNA and the cDNA copy is minimal. B) Syntaxin1 RNAi cells showed a significant reduction of the growth rate expressed as the number of cell divisions within 24 h. Bars standard deviations. C) Stimulated exocytosis of control cells (*n* 50) and (D) Syntaxin1 RNAi cells (*n* 102) of a typical experiment. A picture of a typical cell is shown for each experiment. Stimulated exocytosis of trichocysts is inhibited in Syntaxin1 RNAi cells with most cells show ing no trichocyst discharge. The extent of stimulated trichocyst exocytosis was mea sured per cell and cells of each category were scored; hence, no error bars are shown. Size bar 10 µm. E) Effect of Syntaxin1 RNAi on cell shape. Silenced cells appear smaller and thinner, with the width/length ratio significantly affected (F). Bars standard deviations.

Pt*Syx5—a candidate Golgi marker*

The Golgi apparatus in *Paramecium* consists of several hundreds of dictyosomes, each ~1 µm in size, scattered throughout the cell (65,66). Yet no molecular data were known. We now identified *Pt*Syx5 as a putative marker of the Golgi apparatus of *Paramecium* for the following reasons. (i) Phylogenetic analysis clearly allocates *Pt*Syx5 to the clade of the syntaxin 5 family that mediate transport into and across the Golgi (67–69), the transport from the early recycling endosome to the TGN (70) and the reassembly of Golgi cisternae from mitotic fragments (71). (ii) The fluorescence signal observed in cells transfected with GFP-*Pt*Syx5-1 (Figure 9A–D) is compatible with size and distribution of the Golgi fields in *Paramecium* (65,66). (iii) Treatment with BFA, a well-established inhibitor of Golgi dynamics (43), causes the complete, but reversible breakdown of the distinct GFP-labelled structures (Figure 11B–D). Similar observations were made for the R-SNARE *Pt*Sec22 that is involved in ER-Golgi transport (Figure 11 E–G). Because of the evolutionary distant position of *Paramecium* compared to animals, it is not at all surprising that the pharmacology differs and higher doses of BFA had to be used in accordance with findings in plants (44).

It still has to be examined whether the two putative Golgi paralogues in *Paramecium*, *Pt*Syx5-1 and *Pt*Syx5-2, may serve differential functions. For instance, in the rat liver, a second syntaxin 5 isoform contains an N-terminal ER

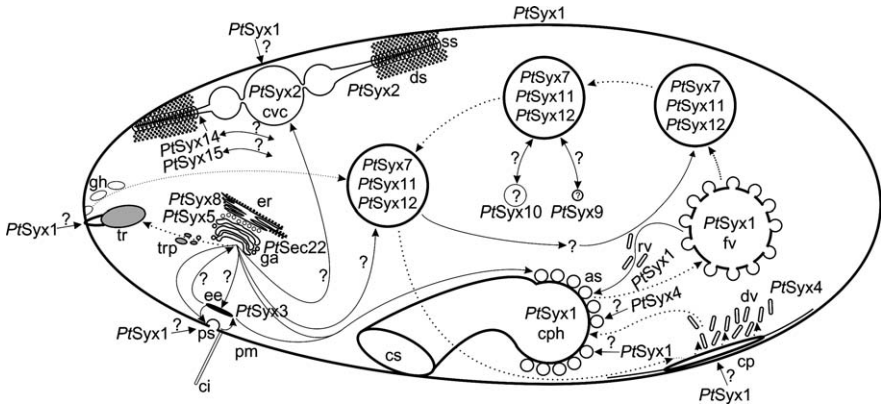

Figure 16: *Paramecium* trafficking network [based mainly on work by Allen and Fok, (14)] superimposed with syntaxin distribution (this article). As there is no indication of a functional or topological diversification within subfamily members at the moment, only the syntaxin subfamily number is indicated. Dotted lines mark the path of organelles, whereas continuous arrows mark vesicle delivery pathways. '?' Indicates putative trafficking pathways for which syntaxin involvement has not been demonstrated so far. For comparison, the localization of *Pt*Sec22 is also indicated. as, acidosome; ci, cilium; cp, cytoproct; cph, cytopharynx; cs, cytostome; cvc, contractile vacuole complex; ds, decorated spongiome of the cvc; dv, discoidal vesicle; ee, early endosome (terminal cisterna); er, endoplasmic reticulum; fv, food vacuole; ga, golgi apparatus; gh, ghost; pm, plasma membrane; ps, parasomal sac (coated pit); ss, smooth spongiome of the cvc; tr, trichocyst; trp, trichocyst precursor.

retrieval signal (55) and in *A. thaliana* several Qa-SNAREs occur in the Golgi apparatus and TGN (51,72).

Phagocytosis-associated syntaxins appear to be a unique clade of Q-SNAREs

According to the evolutionary relationship tree, a large group of *Paramecium* syntaxins, the members of the subfamilies *Pt*Syx7, *Pt*Syx9, *Pt*Syx10, *Pt*Syx11 and *Pt*Syx12, seem to represent a unique clade of Q-SNAREs without having any orthologues in metazoan cells (Figure 3). Because the *Tetrahymena* genome does contain close orthologues, it can be assumed that the syntaxins of this clade may have a role in a more specialized pathway of ciliates and other free-living cells, e.g. in their phagosomal system for food uptake (14,73,74). In *Paramecium*, this is a membrane trafficking system of great complexity (14), where phagosomes sequentially fuse with a series of endomembrane compartments to acquire degradative properties, before their indigestible waste material is expelled. Because this includes acidification and neutralization, fusion with lysosomes and retrieval of membranes, it had to be expected that a high number of syntaxin paralogues might be required. Our *in vivo* GFP localization data clearly support this hypothesis insofar as different Qa-SNAREs are present in different stages of phagosome maturation (Figures 13 and 16). With the identification and assignment of individual syntaxins to this pathway, it will be possible in the future to dissect and analyse individual steps of this pathway in more detail.

Conclusions

The present study enabled us to assign most of the identified syntaxins to different trafficking pathways in the *Paramecium* cell. A promising candidate for exocytosis, a process we are most interested in, could be identified and will be investigated in more detail in future work. Another interesting topic will be to define the targeting signals in *Paramecium* syntaxins and to compare them with proposed localization signals in other systems (75–77). To refine such analysis, *Paramecium* appears appropriate because of its complex membrane trafficking system.

Materials and Methods

Cell culture

Wild type strains of *P. tetraurelia* used were stocks *7S* and *d4 2*, derived from stock *51S* (78). Cells were cultivated in a bacterized medium as described previously (79).

Annotation and characterization of Pt*syx genes*

In order to identify new syntaxin genes in *Paramecium* (*Ptsyx*) by homology searches, the developing *Paramecium* database (http://aiaia.cgm.cnrs gif.fr) was screened by using the nucleotide and amino acid sequence of syntaxins either from other organisms or from already annotated *Parame cium Ptsyx* genes. Positive hits were further analysed by performing blast searches at the National Centre for Biotechnology Information database (80). Conserved motif searches were performed with either PROSITE (81) or with BLAST RPS using pfam entries of the corresponding Conserved Domain Database (82,83). We also used PSIPRED (84) and MEMSAT 2 (85,86), two methods for secondary structure and transmembrane topology pre diction, respectively, included at the server at http://bioinf.cs.ucl.ac.uk/psipred/(87). Phylogenetic and molecular evolutionary analyses were performed with either CLUSTALW or the MEGA version 3 program (88).

Polymerase chain reaction of genomic DNA and cDNAs

Total wild type DNA from strain *7S* for PCR was prepared from log phase cultures as published by Godiska et al. (89). The open reading frames of

individual *Ptsyx* genes were amplified by RT PCR using total RNA prepared according to Haynes et al. (90). Reverse transcriptase polymerase chain reaction was performed in a programmable thermocycler T3 (Biometra, Göttingen, Germany) using 3′oligo dTT primer and the SuperScript™ III reverse transcriptase (Invitrogen, Karlsruhe, Germany) for first strand cDNA synthesis. 3′oligo dTT primer: 5′ AACTGGAAGAATTCGCGGCCGCG GAATTTTTTTTTTTTT 3′. The subsequent PCR (50 μL) was performed with the Advantage 2 cDNA polymerase mix (Clontech, Palo Alto, CA, USA) using *Ptsyx* specific oligonucleotides (Table S1) with or without artificial restriction sites added at their ends. In general, amplifications were performed with one cycle of denaturation (95°C, 1 min), 40 42 cycles of denaturation (95°C, 30 seconds), annealing (54 58°C, 45 seconds) and extension (68°C, 3 min), followed by a final extension step at 68°C for 5 min. Polymerase chain reaction products were sub cloned into the plasmid pCR2.1 by using the TOPO TA™ Cloning Kit (Invitrogen) according to the manufacturer's instructions. After transformation into *Escherichia coli* (DH5 cells or TOP10F′ cells), positive clones were sequenced as described below.

Sequencing

Sequencing was performed by MWG Biotech (Martinsried, Germany) custom sequencing service. DNA sequences were aligned by the CLUSTALW feature integrated in the DNASTAR LASERGENE software package (Madison, WI, USA).

Construction and microinjection of GFP expression plasmids

Ptsyx and *Ptsec22* specific PCR products obtained with the oligonucleotides listed in Table S2 were cloned into the eGFP expression plasmid pPXV GFP (38) either in front of the *egfp* gene, as described by Wassmer et al. (91) or at the end of the *egfp* gene between one of the restriction sites *Nhe*I, *Spe*I or *Pst*I, and the *Xho*I site, respectively, of the plasmid using conventional cloning procedures (92). For microinjection of cells, the pPXV GFP fusion plasmids were linearized with *Sfi*I, which cuts in between the *T. thermophila* inverted telomeric repeats, thus helping to stabilize the DNA in the macronucleus after injection (93). DNA to be injected was isopropanol precipitated and resuspended to a concentration of 1 5 μg/μL in MilliQ water. For microinjection, we used post autogamous cells, which were allowed to grow for 3 4 generations in bacterized salad medium. To avoid any disturbances of the transformation process, cells were also treated with 0.02% aminoethyldextran (to remove trichocysts) and equilibrated in Dryls buffer [2 mM sodium citrate, 1 mM NaH_2PO_4, 1 mM Na_2HPO_4, 1.5 mM $CaCl_2$, pH 6.8; (94)] supplemented with 0.2% BSA. DNA microinjections were made with glass microcapillaries under an Axiovert 100TV phase contrast micro scope (Zeiss, Oberkochen, Germany). Expression of GFP fusion proteins in clonal descendants of microinjected cells was analysed after 16 48 h, either by epifluorescence microscopy in a Axiovert 100TV microscope equipped with GFP filter set 13, a plan Neofluar × 40 oil immersion objective (numeric aperture 1.30) and with a ProgRes C10 plus camera system from Jenoptik (Jena, Germany), or by a conventional LM Axiovert 200M microscope equipped with GFP filter set 38, an alpha plan Neofluar × 40 objective, and with a AxioCam MR camera system (all microscopical equipment from Zeiss). Excitation light was produced by a 100W HBO lamp. Images were processed either with the AXIOVISION software (Zeiss) or with ADOBE PHOTOSHOP (Adobe Systems, San Jose, CA, USA).

Gene silencing by feeding

The coding sequences of individual *Ptsyx* genes, either as ~300 bp isoform specific fragments from genomic DNA or as full length cDNA sequence, were amplified by PCR using *Ptsyx* specific oligonucleotides (Table S3) and cloned into the double T7 promotor plasmid pL4440 (95) via the *Xba*I/*Xho*I or *Hind*III/*Xho*I restriction sites. Plasmids were introduced in the *Escher ichia coli* Ht115 strain and *Paramecium* cells were fed with these strains as described in detail by Wassmer et al. (91). The *Paramecium* cells were analysed after 36 48 h of feeding. Capability of trichocyst exocytosis was routinely tested with a saturated solution of picric acid (96).

Expression of a Pt*Syx1-1-specific peptide in E. coli*

For heterologous expression of a *Pt*Syx specific peptide, we selected a part of the coding region of *Pt*Syx1 1 (I82 I210; accession number CR855934). After changing all deviating *Paramecium* glutamine codons (TAA and TAG) into universal glutamine codons (CAA and CAG) by PCR methods (97) (for primers, see Table S3), this region of *Ptsyx1 1* was cloned into the *Nco*I/*Xho*I restriction sites of the pRV11 expression vector (98), a derivate of the pET System from Novagen (Madison, WI, USA) which adds a 10 amino acid peptide to the C terminus of the selected sequence including a His_6 tag for purification of the recombinant peptides.

Purification of a recombinant Pt*Syx1-1 peptide and preparation of polyclonal antibodies*

The recombinant *Pt*Syx peptide, *Pt*Syx1 $1_{I82\ I210}$, was purified by affinity chromatography on Ni^{2+} nitrilotriacetate agarose under denaturing condi tions, as recommended by the manufacturer (Novagen). The recombinant peptide was eluted with a buffer at pH 4.5 containing 100 mM NaH_2P0_4, 10 mM Trizma base supplemented with 8 M urea and 1 M imidazole. The collected fractions were analysed on SDS polyacrylamide gels, and those containing the recombinant peptides were pooled, dialyzed against PBS and used for immunization of a rabbit. After several boosts, positive sera were taken and affinity purified by two subsequent chromatography steps as described previously (79).

Cell fractionation

For subcellular fractionation, cells were grown in an axenic culture medium at 25°C and harvested at the late logarithmic phase as previously described (99). Whole cell homogenates were prepared in 20 mM phase buffer (20 mM Tris maleate, 20 mM NaOH, 20 mM NaCl and 250 mM sucrose, pH 7.0) as described (79). Soluble and particulate fractions were separated by centrifugation at 100 000 × *g* for 60 min at 4°C. Cell surface complexes (cortices) were prepared according to Lumpert et al. (100), and enriched microsomes according to Kissmehl et al. (101). A protease inhibitor cock tail containing 15 μM pepstatin A, 100 mU/mL aprotinin, 100 μM leupeptin, 0.26 mM Nα (p toluene sulfonyl) L arginine methyl ester, 28 μM E64 and 0.2 mM Pefabloc SC was used throughout.

SDS–PAGE and immunoblotting

Protein samples were denatured by boiling for 5 min in SDS sample buffer, subjected to electrophoresis in 10% SDS polyacrylamide gels using a discontinuous buffer system described before (25). Electroblotting onto nitrocellulose membranes and immunobinding was carried out as described (79) by using affinity purified antibodies against *Pt*Syx1 1. Bound antibodies were detected with a peroxidase conjugated secondary antibody (anti rabbit IgG) (Dianova, Hamburg, Germany) using the Amersham enhanced chemiluminescence detection system.

Brefeldin A treatment of Paramecium cells

A stock solution of 5 μg/μL BFA (Molecular Probes, Eugene, OR, USA) was made in dimethyl sulphoxide (DMSO). Paramecia were incubated in glass depression wells with BFA dilutions ranging in the concentration from 50 ng/ μL to 150 ng/μL for 0 5 h. Control cells were incubated with the same concentration of DMSO. At various time points, living cells were analysed for GFP fluorescence. To show reversibility of the effect, cells were washed in buffer, transferred back to bacterized medium and re analysed after 16 h.

Immuno-LM analysis

Immuno light microscopic analyses were performed either with permeabi lized cells or with isolated cortices. Cells suspended in Pipes/HCl buffer (5 mM, pH 7.2) with 1 mM KCl and 1 mM $CaCl_2$ were fixed in 8% (wt/v) freshly depolymerized formaldehyde in the same buffer solution plus 0.5% digitonin (Sigma, Taufkirchen, Germany), 30 min, 20°C, washed in PBS and then incubated twice in PBS supplemented with 50 mM glycine and finally in PBS plus 1% BSA. The same was performed with isolated corti ces, but without digitonin. Samples were then exposed to affinity purified anti *Pt*Syx1 1 antibodies (1:50), followed by AlexaFluor® 488 conjugated

anti rabbit antibodies (Molecular Probes), the latter diluted 1:100 in PBS + 1% BSA. For controls, either preimmune serum was used or primary antibodies were omitted. Samples were mounted with Mowiol supplemented with *n* propylgallate to reduce fading. Fluorescence was analysed in a confocal laser scanning microscope LSM 510 Meta (Zeiss) equipped with a Plan Apochromat × 63 oil immersion objective (NA 1.4) or in a conventional epifluorescence microscope described above. Images acquired with the LSM 510 software were processed with PHOTOSHOP software (Adobe Systems).

Immuno-EM analysis

Paramecium cells transformed with GFP *Pt*Syx1 1, GFP *Pt*Syx5 1 or GFP *Pt*Sec22 were fixed in 4% formaldehyde plus 0.15% glutaraldehyde in 100 mM cacodylate buffer pH 7.0 for 2.5 h at room temperature, followed by two washes with the same buffer. Cells were dehydrated in ethanol series and embedded in LR Gold resin (Agar Scientifique, Stansted, UK) according to standard protocols. Sections were incubated with anti GFP antibodies (102), followed by protein A bound to colloidal gold particles of 3 or 5 nm size (pA $Au_{3/5}$), and stained with aqueous uranyl acetate and analysed, all as previously described (79).

Acknowledgments

We would like to thank Genoscope (Paris) as well as Drs L. Sperling and J. Cohen (Gif sur Yvette) for access to the server with the sequencing data, Drs C. Stuermer and N. Kasielke for access to and operating the Axiovert 200M, Dr E. May of the Bürkle lab for access to LSM 510 Meta as well as Dr J. Hentschel and D. Bliestle for electronic image processing. This work has been supported by Deutsche Forschungsgemeinschaft (grants to H. P. and R. K. and project C4 of TR SFB11, grant to H. P.)

Supplementary Materials

Figure S1: Treatment of cells with Brefeldin A had no effect on the subcellular localization of *Pt*Syx2 in the contractile vacuole system. Cells were treated with brefeldin, fixed and permeabilized as described in 'Materials and Methods' section. Immunostaining was performed with an affinity purified anti *Pt*Syx2 rabbit antibody and secondary AlexaFluor 488 coupled goat anti rabbit (Molecular Probes). No difference in the staining pattern of *Pt*Syx2 was found between control cells treated with the same concentration of solvent and brefeldin A treated cells. Bar = 10 μm.

Table S1: Oligonucleotides used to study syntaxin gene expression (cDNA).

Table S2: Oligonucleotides used to amplify syntaxin for GFP tagging at the C-terminus (C) or N-terminus (N).

Table S3: Oligonucleotides for heterologous expression of His-tagged *Pt*Syx1-1 peptide I_{82}–I_{210} in *Escherichia coli*.

Supplemental materials are available as part of the online article at http://www.blackwell synergy.com

References

1. Chen YA, Scheller RH. SNARE mediated membrane fusion. Nat Rev Mol Cell Biol 2001;2:98 106.
2. Ungar D, Hughson FM. SNARE protein structure and function. Annu Rev Cell Dev Biol 2003;19:493 517.
3. Hong W. SNAREs and traffic. Biochim Biophys Acta 2005;1744: 120 144.
4. Söllner T, Bennett MK, Whiteheart SW, Scheller RH, Rothman JE. A protein assembly disassembly pathway in vitro that may correspond to sequential steps of synaptic vesicle docking, activation, and fusion. Cell 1993;75:409 418.
5. Weber T, Zemelman BV, McNew JA, Westermann B, Gmachl M, Parlati F, Söllner TH, Rothman JE. SNAREpins: minimal machinery for membrane fusion. Cell 1998;92:759 772.
6. Hanson PI, Heuser JE, Jahn R. Neurotransmitter release four years of SNARE complexes. Curr Opin Neurobiol 1997;7:310 315.
7. Sutton RB, Fasshauer D, Jahn R, Brunger AT. Crystal structure of a SNARE complex involved in synaptic exocytosis at 2.4 A resolution. Nature 1998;395:347 353.
8. Poirier MA, Xiao W, Macosko JC, Chan C, Shin YK, Bennett MK. The synaptic SNARE complex is a parallel four stranded helical bundle. Nat Struct Biol 1998;5:765 769.
9. Katz L, Brennwald P. Testing the 3Q:1R ''rule'': mutational analysis of the ionic ''zero'' layer in the yeast exocytic SNARE complex reveals no requirement for arginine. Mol Biol Cell 2000;11:3849 3858.
10. Fasshauer D, Sutton RB, Brunger AT, Jahn R. Conserved structural features of the synaptic fusion complex: SNARE proteins reclassi fied as Q and R SNAREs. Proc Natl Acad Sci U S A 1998;95: 15781 15786.
11. Bock JB, Matern HT, Peden AA, Scheller RH. A genomic perspective on membrane compartment organization. Nature 2001;409:839 841.
12. Fukuda R, McNew JA, Weber T, Parlati F, Engel T, Nickel W, Rothman JE, Sollner TH. Functional architecture of an intracellular membrane t SNARE. Nature 2000;407:198 202.
13. Burri L, Lithgow T. A complete set of SNAREs in yeast. Traffic 2004;5:45 52.
14. Allen RD, Fok AK. Membrane trafficking and processing in *Parame cium*. Int Rev Cytol 2000;198:277 318.
15. Plattner H, Kissmehl R. Molecular aspects of membrane trafficking in *Paramecium*. Int Rev Cytol 2003;232:185 216.
16. Allen RD, Schroeder CC, Fok AK. Endosomal system of *Paramecium*: coated pits to early endosomes. J Cell Sci 1992;101:449 461.
17. Elde NC, Morgan G, Winey M, Sperling L, Turkewitz AP. Elucidation of clathrin mediated endocytosis in *TETRAHYMENA* reveals an evolu tionarily convergent recruitment of dynamin. PLoS Genet 2005;1:e52.
18. Flötenmeyer M, Momayezi M, Plattner H. Immunolabeling analysis of biosynthetic and degradative pathways of cell surface components (glycocalyx) in *Paramecium* cells. Eur J Cell Biol 1999;78:67 77.
19. Vayssié L, Skouri F, Sperling L, Cohen J. Molecular genetics of regulated secretion in *Paramecium*. Biochimie 2000;82:269 288.
20. Plattner H, Kissmehl R. Dense core secretory vesicle docking and exocytotic membrane fusion in *Paramecium* cells. Biochim Biophys Acta 2003;1641:183 193.
21. Allen RD. Food vacuole membrane growth with microtubule associ ated membrane transport in *Paramecium*. J Cell Biol 1974;63: 904 922.
22. Allen RD, Naitoh Y. Osmoregulation and contractile vacuoles of protozoa. Int Rev Cytol 2002;215:351 394.
23. Allen RD. The contractile vacuole and its membrane dynamics. Bioessays 2000;22:1035 1042.
24. Froissard M, Kissmehl R, Dedieu JC, Gulik Krzywicki T, Plattner H, Cohen J. N ethylmaleimide sensitive factor is required to organize functional exocytotic microdomains in *Paramecium*. Genetics 2002; 161:643 650.
25. Kissmehl R, Froissard M, Plattner H, Momayezi M, Cohen J. NSF regulates membrane traffic along multiple pathways in *Paramecium*. J Cell Sci 2002;115:3935 3946.
26. Schilde C, Wassmer T, Mansfeld J, Plattner H, Kissmehl R. A multigene family encoding R SNAREs in the ciliate *Paramecium* tetraurelia. Traffic 2006;7:440 455.

27. Aury JM, Jaillon O, Duret L, Noel B, Jubin C, Porcel BM, Segurens B, Daubin V, Anthouard V, Aiach N, Arnaiz O, Billaut A, Beisson J, Blanc I, Bouhouche K, et al. Global trends of whole genome duplications revealed by the ciliate *Paramecium tetraurelia*. Nature 2006;444: 171 178.
28. Russell CB, Fraga D, Hinrichsen RD. Extremely short 20 33 nucleo tide introns are the standard length in *Paramecium tetraurelia*. Nucleic Acids Res 1994;22:1221 1225.
29. Sperling L, Dessen P, Zagulski M, Pearlman RE, Migdalski A, Gromadka R, Froissard M, Keller AM, Cohen J. Random sequencing of *Paramecium* somatic DNA. Eukaryot Cell 2002;1:341 352.
30. Teng FY, Wang Y, Tang BL. The syntaxins. Genome Biol 2001;2: REVIEWS3012.
31. Salaun C, James DJ, Greaves J, Chamberlain LH. Plasma membrane targeting of exocytic SNARE proteins. Biochim Biophys Acta 2004; 1693:81 89.
32. Misura KM, Bock JB, Gonzalez LC Jr, Scheller RH, Weis WI. Three dimensional structure of the amino terminal domain of syntaxin 6, a SNAP 25 C homolog. Proc Natl Acad Sci U S A 2002;99: 9184 9189.
33. Antonin W, Fasshauer D, Becker S, Jahn R, Schneider TR. Crystal structure of the endosomal SNARE complex reveals common struc tural principles of all SNAREs. Nat Struct Biol 2002;9:107 111.
34. Subramaniam VN, Loh E, Horstmann H, Habermann A, Xu Y, Coe J, Griffiths G, Hong W. Preferential association of syntaxin 8 with the early endosome. J Cell Sci 2000;113:997 1008.
35. Jahn R, Lang T, Südhof TC. Membrane fusion. Cell 2003;112:519 533.
36. Fernandez I, Ubach J, Dulubova I, Zhang X, Sudhof TC, Rizo J. Three dimensional structure of an evolutionarily conserved N terminal domain of syntaxin 1A. Cell 1998;94:841 849.
37. Misura KM, Scheller RH, Weis WI. Self association of the H3 region of syntaxin 1A. Implications for intermediates in SNARE complex assembly. J Biol Chem 2001;276:13273 13282.
38. Hauser K, Haynes WJ, Kung C, Plattner H, Kissmehl R. Expression of the green fluorescent protein in *Paramecium tetraurelia*. Eur J Cell Biol 2000;79:144 149.
39. Apodaca G, Cardone MH, Whiteheart SW, DasGupta BR, Mostov KE. Reconstitution of transcytosis in SLO permeabilized MDCK cells: existence of an NSF dependent fusion mechanism with the apical surface of MDCK cells. EMBO J 1996;15:1471 1481.
40. Low SH, Chapin SJ, Weimbs T, Komuves LG, Bennett MK, Mostov KE. Differential localization of syntaxin isoforms in polarized Madin Darby canine kidney cells. Mol Biol Cell 1996;7:2007 2018.
41. Newman AP, Shim J, Ferro Novick S. BET1, BOS1, and SEC22 are members of a group of interacting yeast genes required for transport from the endoplasmic reticulum to the Golgi complex. Mol Cell Biol 1990;10:3405 3414.
42. Lewis MJ, Pelham HR. SNARE mediated retrograde traffic from the Golgi complex to the endoplasmic reticulum. Cell 1996;85:205 215.
43. Klausner RD, Donaldson JG, Lippincott Schwartz J. Brefeldin A: insights into the control of membrane traffic and organelle structure. J Cell Biol 1992;116:1071 1080.
44. Moreau P, Brandizzi F, Hanton S, Chatre L, Melser S, Hawes C, Satiat Jeunemaitre B. The plant ER Golgi interface: a highly structured and dynamic membrane complex. J Exp Bot 2007;58:49 64.
45. Ramoino P, Diaspro A, Fato M, Beltrame F, Robello M. Changes in the endoplasmic reticulum structure of *Paramecium primaurelia* in rela tion to different cellular physiological states. J Photochem Photobiol B 2000;54:35 42.
46. Hauser K, Pavlovic N, Klauke N, Geissinger D, Plattner H. Green fluorescent protein tagged sarco(endo)plasmic reticulum Ca^{2+} ATPase overexpression in *Paramecium* cells: isoforms, subcellular localization, biogenesis of cortical calcium stores and functional aspects. Mol Microbiol 2000;37:773 787.
47. Kneen M, Farinas J, Li Y, Verkman AS. Green fluorescent protein as a noninvasive intracellular pH indicator. Biophys J 1998;74:1591 1599.
48. Galvani A, Sperling L. RNA interference by feeding in *Paramecium*. Trends Genet 2002;18:11 12.
49. Ruiz F, Vayssié L, Klotz C, Sperling L, Madeddu L. Homology depend ent gene silencing in *Paramecium*. Mol Biol Cell 1998;9:931 943.
50. Dacks JB, Doolittle WF. Molecular and phylogenetic characterization of syntaxin genes from parasitic protozoa. Mol Biochem Parasitol 2004;136:123 136.
51. Uemura T, Ueda T, Ohniwa RL, Nakano A, Takeyasu K, Sato MH. Systematic analysis of SNARE molecules in *Arabidopsis*: dissection of the post Golgi network in plant cells. Cell Struct Funct 2004;29:49 65.
52. Besteiro S, Coombs GH, Mottram JC. The SNARE protein family of *Leishmania major*. BMC Genomics 2006;7:250.
53. Dacks JB, Doolittle WF. Novel syntaxin gene sequences from *Giardia, Trypanosoma* and algae: implications for the ancient evolution of the eukaryotic endomembrane system. J Cell Sci 2002;115:1635 1642.
54. Bennett MK, Garcia Arraras JE, Elferink LA, Peterson K, Fleming AM, Hazuka CD, Scheller RH. The syntaxin family of vesicular transport receptors. Cell 1993;74:863 873.
55. Hui N, Nakamura N, Sonnichsen B, Shima DT, Nilsson T, Warren G. An isoform of the Golgi t SNARE, syntaxin 5, with an endoplasmic reticulum retrieval signal. Mol Biol Cell 1997;8:1777 1787.
56. Quinones B, Riento K, Olkkonen VM, Hardy S, Bennett MK. Syntaxin 2 splice variants exhibit differential expression patterns, biochemical properties and subcellular localizations. J Cell Sci 1999;112: 4291 4304.
57. Scales SJ, Yoo BY, Scheller RH. The ionic layer is required for efficient dissociation of the SNARE complex by alpha SNAP and NSF. Proc Natl Acad Sci U S A 2001;98:14262 14267.
58. Dulubova I, Yamaguchi T, Wang Y, Sudhof TC, Rizo J. Vam3p structure reveals conserved and divergent properties of syntaxins. Nat Struct Biol 2001;8:258 264.
59. Antonin W, Dulubova I, Arac D, Pabst S, Plitzner J, Rizo J, Jahn R. The N terminal domains of syntaxin 7 and vti1b form three helix bundles that differ in their ability to regulate SNARE complex assembly. J Biol Chem 2002;277:36449 36456.
60. Yang B, Steegmaier M., Gonzalez LC Jr, Scheller RH. nSec1 binds a closed conformation of syntaxin1A. J Cell Biol 2000;148:247 252.
61. Schütz D, Zilly F, Lang T, Jahn R, Bruns D. A dual function for Munc 18 in exocytosis of PC12 cells. Eur J Neurosci 2005;21:2419 2432.
62. Tagaya M, Toyonaga S, Takahashi M, Yamamoto A, Fujiwara T, Akagawa K, Moriyama Y, Mizushima S. Syntaxin 1 (HPC 1) is asso ciated with chromaffin granules. J Biol Chem 1995;270:15930 15933.
63. Walch Solimena C, Blasi J, Edelmann L, Chapman ER, von Mollard GF, Jahn R. The t SNAREs syntaxin 1 and SNAP 25 are present on organelles that participate in synaptic vesicle recycling. J Cell Biol 1995;128:637 645.
64. Band AM, Kuismanen E. Localization of plasma membrane t SNAREs syntaxin 2 and 3 in intracellular compartments. BMC Cell Biol 2005; 6:26.
65. Esteve JC. [Golgi apparatus in ciliates. Ultrastructure, with special reference to *Paramecium*]. J Protozool 1972;19:609 618.
66. Allen RD. Cytology. In: Görtz HD, editor. *Paramecium*. Berlin: Springer Verlag; 1988, pp. 4 40.
67. Rowe T, Dascher C, Bannykh S, Plutner H, Balch WE. Role of vesicle associated syntaxin 5 in the assembly of pre Golgi intermedi ates. Science 1998;279:696 700.
68. Roy L, Bergeron JJ, Lavoie C, Hendriks R, Gushue J, Fazel A, Pelletier A, Morre DJ, Subramaniam VN, Hong W, Paiement J. Role of p97 and

syntaxin 5 in the assembly of transitional endoplasmic reticulum. Mol Biol Cell 2000;11:2529 2542.
69. Volchuk A, Ravazzola M, Perrelet A, Eng WS, Di Liberto M, Varlamov O, Fukasawa M, Engel T, Sollner TH, Rothman JE, Orci L. Countercurrent distribution of two distinct SNARE complexes mediating transport within the Golgi stack. Mol Biol Cell 2004;15:1506 1518.
70. Tai G, Lu L, Wang TL, Tang BL, Goud B, Johannes L, Hong W. Participation of the syntaxin 5/Ykt6/GS28/GS15 SNARE complex in transport from the early/recycling endosome to the trans Golgi network. Mol Biol Cell 2004;15:4011 4022.
71. Rabouille C, Kondo H, Newman R, Hui N, Freemont P, Warren G. Syntaxin 5 is a common component of the NSF and p97 mediated reassembly pathways of Golgi cisternae from mitotic Golgi fragments in vitro. Cell 1998;92:603 610.
72. Sanderfoot AA, Kovaleva V, Bassham DC, Raikhel NV. Interactions between syntaxins identify at least five SNARE complexes within the Golgi/prevacuolar system of the *Arabidopsis* cell. Mol Biol Cell 2001;12:3733 3743.
73. Hackam DJ, Rotstein OD, Bennett MK, Klip A, Grinstein S, Manolson MF. Characterization and subcellular localization of target membrane soluble NSF attachment protein receptors (t SNAREs) in macro phages. Syntaxins 2, 3, and 4 are present on phagosomal mem branes. J Immunol 1996;156:4377 4383.
74. Gotthardt D, Warnatz HJ, Henschel O, Bruckert F, Schleicher M, Soldati T. High resolution dissection of phagosome maturation re veals distinct membrane trafficking phases. Mol Biol Cell 2002;13: 3508 3520.
75. Tang BL, Hong W. A possible role of di leucine based motifs in targeting and sorting of the syntaxin family of proteins. FEBS Lett 1999;446:211 212.
76. Kasai K, Akagawa K. Roles of the cytoplasmic and transmembrane domains of syntaxins in intracellular localization and trafficking. J Cell Sci 2001;114:3115 3124.
77. Watson RT, Pessin JE. Transmembrane domain length determines intracellular membrane compartment localization of syntaxins 3, 4, and 5. Am J Physiol Cell Physiol 2001;281:C215 C223.
78. Sonneborn TM. *Paramecium aurelia*. In: Kung RC, editor. Handbook of Genetics. New York: Plenum Press; 1974, pp. 469 594.
79. Kissmehl R, Sehring IM, Wagner E, Plattner H. Immunolocalization of actin in *Paramecium* cells. J Histochem Cytochem 2004;52: 1543 1559.
80. Altschul SF, Madden TL, Schaffer AA, Zhang J, Zhang Z, Miller W, Lipman DJ. Gapped BLAST and PSI BLAST: a new generation of protein database search programs. Nucleic Acid Res 1997;25: 3389 3402.
81. Bairoch A, Bucher P, Hofmann K. The PROSITE database, its status in 1997. Nucleic Acids Res 1997;25:217 221.
82. Marchler Bauer A, Anderson JB, Cherukuri PF, DeWeese Scott C, Geer LY, Gwadz M, He S, Hurwitz DI, Jackson JD, Ke Z, Lanczycki CJ, Liebert CA, Liu C, Lu F, Marchler GH, et al. CDD: a Conserved Domain Database for protein classification. Nucleic Acids Res 2005;33: D192 D196.
83. Bateman A, Coin L, Durbin R, Finn RD, Hollich V, Griffiths Jones S, Khanna A, Marshall M, Moxon S, Sonnhammer EL, Studholme DJ, Yeats C, Eddy SR. The Pfam protein families database. Nucleic Acids Res 2004;32:D138 D141.
84. Jones DT. Protein secondary structure prediction based on position specific scoring matrices. J Mol Biol 1999;292:195 202.
85. Jones DT, Taylor WR, Thornton JM. A model recognition approach to the prediction of all helical membrane protein structure and topology. Biochemistry 1994;33:3038 3049.
86. Jones DT. Do transmembrane protein superfolds exist? FEBS Lett 1998;423:281 285.
87. McGuffin LJ, Bryson K, Jones DT. The PSIPRED protein structure prediction server. Bioinformatics 2000;16:404 405.
88. Kumar S, Tamura K, Nei M. MEGA3: Integrated software for Molecular Evolutionary Genetics Analysis and sequence alignment. Brief Bioinform 2004;5:150 163.
89. Godiska R, Aufderheide KJ, Gilley D, Hendrie P, Fitzwater T, Preer LB, Polisky B, Preer JR Jr. Transformation of *Paramecium* by microinjec tion of a cloned serotype gene. Proc Natl Acad Sci U S A 1987;84: 7590 7594.
90. Haynes WJ, Vaillant B, Preston RR, Saimi Y, Kung C. The cloning by complementation of the pawn A gene in *Paramecium*. Genetics 1998;149:947 957.
91. Wassmer T, Froissard M, Plattner H, Kissmehl R, Cohen J. The vacuolar proton ATPase plays a major role in several membrane bounded organelles in *Paramecium*. J Cell Sci 2005;118:2813 2825.
92. Sambrook J, Fritch E, Maniatis T. Molecular Cloning: A Laboratory Manual. Cold Spring Harbor: Cold Spring Harbor Laboratory Press; 1989.
93. Haynes WJ, Ling KY, Saimi Y, Kung C. Induction of antibiotic resistance in *Paramecium tetraurelia* by the bacterial gene APH 3′ II. J Eukaryot Microbiol 1995;42:83 91.
94. Dryl S. Effect of adaptation to the environment on chemotaxis of *Paramecium caudatum*. Acta Biol Exp 1959;19:83 93.
95. Timmons L, Court DL, Fire A. Ingestion of bacterially expressed dsRNAs can produce specific and potent genetic interference in *Caenorhabditis elegans*. Gene 2001;263:103 112.
96. Pollack S. Mutations affecting the trichocysts in *Paramecium aurelia*. I. Morphology and description of the mutants. J Protozool 1974;21: 352 362.
97. Dillon PJ, Rosen CA. Use of polymerase chain reaction for the rapid construction of synthetic genes. Methods Mol Biol 1993;15:263 s269.
98. Wirsel SGR, Vögele R, Bänninger R, Mendgen KW. Cloning of β tubulin and succinate dehydrogenase genes from *Uromyces fabae* and establishing selection conditions for their use in transformation. Eur J Plant Pathol 2004;110:767 777.
99. Kissmehl R, Treptau T, Hofer HW, Plattner H. Protein phosphatase and kinase activities possibly involved in exocytosis regulation in *Paramecium tetraurelia*. Biochem J 1996;317:65 76.
100. Lumpert CJ, Kersken H, Plattner H. Cell surface complexes ('corti ces') isolated from Paramecium tetraurelia cells as a model system for analysing exocytosis in vitro in conjunction with microinjection studies. Biochem J 1990;269:639 645.
101. Kissmehl R, Huber S, Kottwitz B, Hauser K, Plattner H. Subplasma lemmal Ca stores in Paramecium tetraurelia. Identification and char acterisation of a sarco(endo)plasmic reticulum like $Ca^{(2+)}$ ATPase by phosphoenzyme intermediate formation and its inhibition by caffeine. Cell Calcium 1998;24:193 203.
102. Wassmer T, Kissmehl R, Cohen J, Plattner H. Seventeen a subunit isoforms of *Paramecium* V ATPase provide high specialization in localization and function. Mol Biol Cell 2006;17:917 930.